Mechanism and Machine Theory 126 (2018) 273–294

Contents lists available at ScienceDirect

Mechanism and Machine Theory

journal homepage: www.elsevier.com/locate/mechmachtheory

Research paper

Introducing mass parameters to Pseudo–Rigid–Body models for precisely predicting dynamics of compliant mechanisms☆

Yu She[a,1], Deshan Meng[b,1], Hai-Jun Su[a,*], Siyang Song[a], Junmin Wang[a]

[a] Department of Mechanical and Aerospace Engineering, The Ohio State University, Columbus, OH 43210, United States
[b] Department of Automation, Graduate School at Shenzhen, Tsinghua University, Guangdong, Shenzhen, 518055, PR China

ARTICLE INFO

Article history:
Received 1 January 2018
Revised 22 March 2018
Accepted 6 April 2018
Available online 27 April 2018

Keywords:
Compliant mechanisms
Parallel-guiding mechanisms
Pseudo–Rigid–Body model
Mass property parameters
Continuum model
Dynamics
Natural frequency

ABSTRACT

In this paper, we introduce non-dimensional mass property parameters to the classical PRB model for accurately predicting the dynamics of the compliant mechanisms. Given extensive work on PRB models accurately modeling the statics and kinematics of compliant mechanisms, few works have investigated on their accuracy in predicting dynamics. Here we study the fundamental natural frequency of two typical mechanisms: fixed-root and pinned-root compliant parallel-guiding mechanisms (CPGM). First, analytical expressions of the natural frequencies of the continuum models are derived according to the vibration mechanics. Second, theoretical expressions of the natural frequencies of the parameterized PRB model are obtained from their dynamics equations. Third, the mass property parameters are optimized to minimize the error between the continuum models and the parameterized PRB model. We conclude that the optimized PRB models can well predict the dynamics especially the low input signal frequency or mass of beams are not negligible. These new PRB models can significantly improve computational efficiency in dynamics simulation of compliant mechanisms.

1. Introduction

Compliant mechanisms have numerous applications in mechanical designs [1–3] and robotic systems [4–6] due to their strengths including reduced part count, less friction, and easy for assembly with high precision and reliability [7]. However, compliant mechanisms are relatively difficult in analyzing, designing, and modeling, especially the dynamic modeling due to the infinite degree of freedom (DOF). To address kinetostatic analysis of the compliant mechanisms, finite element analysis (FEA) [8] method and the Pseudo–Rigid–Body (PRB) model [9,10] are two commonly used approaches. In addition, the Chained–Beam–Constraint–Model (CBCM) is recently developed [11,12] for the static analysis of compliant beams. However the FEA method requires significant computational load to obtain an acceptable accuracy. The PRB model method, on the other hand, has been developed and proven as an efficient approach for design and kinetostatic analysis of the compliant mechanisms with a moderate accuracy.

Recent developments of PRB models on statics and kinematics include the 2R PRB model [13], the 3R PRB model [14], the RPR model considering beam extension or beam circular shape [15,16], etc. However, research on the dynamics of the

☆ This work was conducted in The Ohio State University.

* Corresponding author.
E-mail address: su.298@osu.edu (H.-J. Su).

[1] These authors contributed equally to this work.

https://doi.org/10.1016/j.mechmachtheory.2018.04.005
0094-114X/

Nomenclature

A	cross section area of the beam
E	Young's modulus of the material
I	second moment of inertia
$\boldsymbol{K}$	stiffness matrix of the dynamics equation
L	length of the beam
$\boldsymbol{M}$	inertia matrix of the dynamics equation
a	location of the mass center
h	height
m	mass
t	thickness
w	transverse displacement
y	the mode wave number
α	ratio of distance of the mass center to the length
β	ratio of the mass of the PRB segment to the beam mass
γ	characteristic radius factor
δ	the mode frequency error between the continuum model and the simulation model
λ	ratio of the tip mass to the beam mass
ρ	density of the material

Subscripts

b	beam
i	counters
t	beam tip

Superscripts

p	the PRB model
c	the continuum model
s	the simulation model

compliant mechanisms using PRB models is limited and particularly on the accuracy study [17]. Lobontiu [18] studied the dynamics of flexure hinges including kinetic energy, free/forced response, and damping effects. Li and Kota [19] investigated the natural frequency characteristic and the dynamic response of the compliant mechanisms using the FEA method. Rösner et al. [20] derived a dynamic model of flexure hinges via the FEA method. Zhao et al. [21] developed the dynamic model of a compliant linear-motion mechanism using the Lagrange equation. In addition to the traditional approaches on dynamic analysis, a few studies have investigated the PRB model on dynamic analysis of compliant mechanisms. Boyle et al. [22] presented the dynamics of a constant-force compliant mechanism with a generalized PRB model, but effects of the input signal's parameters and the design parameters are relatively less explored. Yu et al. [23] studied the dynamics of the PRB model of the compliant mechanisms, and Lyon et al. [24,25] studied the first modal frequency of compliant mechanisms based on the PRB model. However, both of them only studied the natural frequencies and no dynamic performance and accuracy were investigated. She et al. [26] studied the dynamics of the 3R PRB model, but the accuracy of dynamics of the PRB model only held for a short time period and no explorations were conducted on the effects of the design or input parameters on the output performance or accuracy. She et al. [27] first introduced mass property parameters to the original PRB model, but the work was limited to the optimization of the fundamental natural frequency, and no dynamic performance was explored. Li et al. [28] investigated the dynamics of the PRB model considering the design parameters such as the mass ratio of the beam mass over the end mass. However, they did not derive the analytical expression of the natural frequency in terms of design parameters.

In this paper, we present a systematical procedure for developing optimized PRB models that can precisely predict the dynamics of compliant mechanisms. We introduce a set of mass property parameters to the classical PRB model such that the fundamental natural frequency of the optimized PRB model agrees with that of the continuum model. The organization of the paper is described as the following. We begin with the problem statement in Section 2. Theoretical expressions of the continuum model with its natural frequency are derived in Section 3. Parametrized PRB models with analytical expressions of the natural frequency of the compliant beams are presented in Section 4. Dynamics validations and evaluations are conducted in Section 5. Finally, conclusions and future work are presented in Section 6.

2. The problem statement

It is well known that the conventional PRB models predict the static force deflection of a flexible continuum member using a serial chain of two or more rigid links joined by torsion/extension springs [29]. In these PRB models, two sets

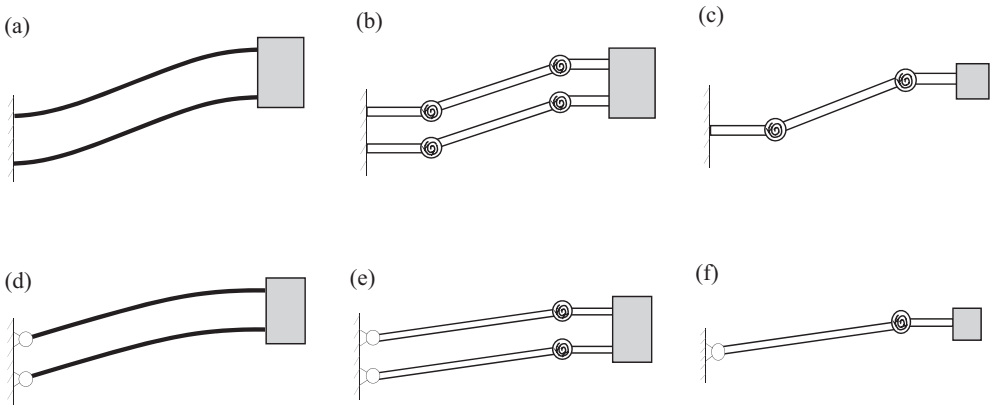

Fig. 1. (a) A fixed-root compliant parallel-guiding mechanism, (b) the PRB model of the fixed-root compliant parallel-guiding mechanism, (c) the PRB model for a fixed-guided beam, (d) A pinned-root compliant parallel-guiding mechanism, (e) the PRB model of the pinned-root compliant parallel-guiding mechanism, (f) the PRB model for a pinned-guided beam.

of parameters: kinematic parameters (e.g. characteristic length, tip deflection coefficient) and compliance parameters (e.g. torsion/extension spring constants) were obtained by minimizing errors between the PRB model and the continuum model calculated either by beam theories or finite element simulations.

One of the most important factors affecting dynamics of a mechanical system is the natural frequency, which is determined by boundary conditions, effective stiffness and effective mass. A general calculation of the natural frequency for a mass-spring system may be expressed as:

$$f = \frac{1}{2\pi}\sqrt{\frac{K}{M}}, \tag{1}$$

where K is the stiffness and M is the mass of the system.

Given the dynamic equations of the PRB model of a compliant mechanism, one can calculate the natural frequency of the PRB model according to Eq. (1). Meanwhile, the natural frequency of a compliant beam can be obtained by studying the continuum model with an analytical expression. Since both of them have theoretical expressions, the natural frequency of the PRB model may be optimized to agree with that of the continuum model. Specifically, non-dimensional mass property parameters will be introduced to the original PRB model, and are then optimized. This framework is a generalized approach and can be applied to any compliant mechanisms as long as the corresponding PRB models are specified and the boundary conditions and design parameters are confirmed. Compliant parallel-guiding mechanism (CPGM) is a typical compliant mechanism with one DOF providing accurate linear motion capabilities [30], and complex mechanical devices can be designed by combining individuals in parallel and/or series [31]. In this paper, CPGM will be studied as a case to verification. In particular, we study CPGM with two typical boundary conditions: fixed-root (Fig. 1(a)) and pinned-root (Fig. 1(b)).

The conventional PRB models for the fixed-root and the pinned-root CPGM are shown in Fig. 1(b) and (d), respectively. To simplify the analysis procedure, we only need to study half of these PRB models, i.e. PRB models of a single beam with two different boundary conditions, as shown in Fig. 1(c) and (f). The full model and the half model have the same natural frequency verified by FEA simulations.

In what follows, continuum models of a compliant beam with the fixed-guided and pinned-guided boundary conditions will be first studied. Then parameterized PRB models of the fixed-guided and pinned-guided compliant beam will be developed and optimized. Finally, the optimized PRB models will be validated by FEA simulations from both of the time domain and the frequency domain, and the effects of the input and design parameters on dynamics will be explored as well.

3. Analytical continuum models of compliant beams

In this section, we derive theoretical expressions of the natural frequencies of the continuum model of both the fixed-guided and pinned-guided compliant beams and validate them by FEA simulation.

3.1. The fixed-guided compliant beam

Considering a fixed-guided compliant beam with a tip load as shown in Fig. 2(a), the beam has a length of L, a cross area of A, an area moment of inertia of I, a density of ρ, and a tip mass of m_t. For convenient analysis, here we start the derivation from a linear continuum model. The governing differential equation of the transverse displacement $w(x, t)$ may be described as:

$$EI\frac{\partial^4 w(x,t)}{\partial x^4} + \rho A\frac{\partial^2 w(x,t)}{\partial t^2} = 0 \tag{2}$$

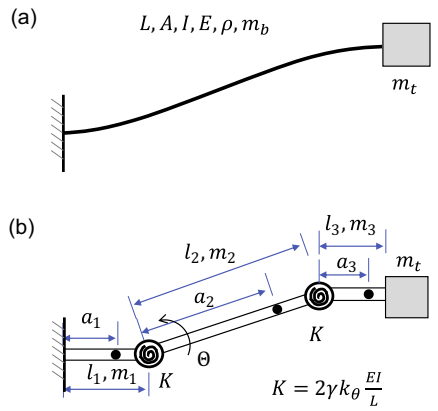

Fig. 2. (a) A fixed-guided compliant beam with a tip load, (b) its parameterized PRB model.

The solution of the above governing equation has the following form:

$$w(x) = C_1 \sin(\phi x) + C_2 \cos(\phi x) + C_3 \sinh(\phi x) + C_4 \cosh(\phi x), \tag{3}$$

where ϕ is the wave number, and C_i are constant coefficients.

Given the boundary conditions of the fixed-guided compliant beam, there is no displacement and angular rotation at the beam root and no angular rotation at the beam tip. The shear force at the tip should be considered since we consider a tip mass placed at the beam tip [32]. Therefore, the boundary conditions of the fixed-guided compliant beam with a tip load can be expressed as:

$$\begin{cases} w(0,t) = 0 \\ \dfrac{\partial w(0,t)}{\partial x} = 0 \\ \dfrac{\partial w(L,t)}{\partial x} = 0 \\ EI\dfrac{\partial^3 w(L,t)}{\partial x^3} = m_t \dfrac{\partial^2 w(L,t)}{\partial t^2} \end{cases} \tag{4}$$

Substituting Eq. (4) to Eq. (3) yields the following transcendental equation in order to achieve a nontrivial solution:

$$\frac{1}{y}\frac{2(\sin y \cosh y + \cos y \sinh y)}{1 + \cosh^2 y - \sinh^2 y - 2\cos y \cosh y} = \lambda, \tag{5}$$

where y is the dimensioned wave number, and it is a variable with respect to the mass parameters, and λ is defined as the mass ratio of the tip mass (m_t) over the beam mass (m_b):

$$\lambda = \frac{m_t}{m_b}. \tag{6}$$

Given any specific design of λ, one may solve Eq. (5) for y. Note Eq. (5) has an infinite number of solutions. Here we only show the first three in Table 5 in the Appendix A. It is observed that y decreases as the increasing of λ. In addition, y decreases rapidly for $\lambda \in [0, 10]$ while only gently for $\lambda \in [100,1E+6]$. That means, the mass ratio does not play a key role for large λ, i.e. the beam mass does not significantly affect the natural frequency if the tip mass dominates the dynamics.

With the solution of y, one can analytically calculate the natural frequencies of the fixed-guided compliant beam based on the continuum model:

$${}^c f_i(\lambda) = \frac{1}{2\pi}\left(\frac{y_i(\lambda)}{L}\right)^2 \sqrt{\frac{EI}{\rho A}}, \quad i = 1, 2, 3, \cdots n. \tag{7}$$

where i is the mode number and superscript c represents the continuum model. By factoring out the physical parameters, a simplified form of the natural frequency can be obtained as:

$${}^c \bar{f}_i(\lambda) = {}^c f_i(\lambda)\left(2\pi L^2 \sqrt{\frac{\rho A}{EI}}\right) = y_i^2(\lambda), \quad i = 1, 2, 3, \cdots n. \tag{8}$$

Table 1
Parameters of the fixed-guided cantilever beam.

Parameter	Value
Young's Modulus	$E = 69\,\text{GPa}$
Density of beam	$\rho = 2700\,\text{kg m}^{-1}$
Poisson ratio	$\nu = 0.3$
Length	$L = 0.225\,\text{m}$
Thickness	$t = 0.001\,\text{m}$
Height	$h = 0.073\,\text{m}$

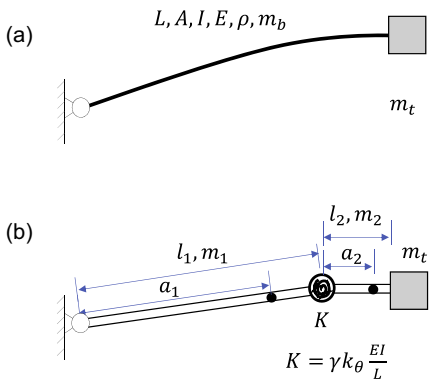

Fig. 3. (a) A pinned-guided compliant beam with a tip load, (b) its parameterized PRB model.

To validate the continuum model, simulations in Abaqus FEA have been conducted. We define the error of the ith modal natural frequency between the continuum model and FEA simulations as:

$$\delta_i = \left| \frac{{}^s f_i - {}^c f_i}{{}^s f_i} \right| \times 100\%, \quad i = 1, 2, 3, \cdots n. \tag{9}$$

where superscript s represents the FEA model. With the physical parameters in Table 1, the calculation and simulation results are shown in Table 6 in Appendix A.

We can see that the errors are very small for all of the three modal natural frequencies for all cases of different mass ratios of λ. We conclude that the analytical continuum model is validated. We can also draw the following conclusions by observation. First, the natural frequency decreases along with the increasing of λ. That is, a heavy mass load results in a small natural frequency, which agrees with our intuition. Second, the natural frequency decreases rapidly for $\lambda \in [0, 10]$ while only gently for $\lambda \in$ [100,1E+6]. The first modal natural frequency continuously decreases for $\lambda \in$ [100,1E+6] while the second and third modal natural frequency converge to constant values. Furthermore, it shows that the higher modal natural frequencies correspond to larger errors. Finally, it seems that λ has no obvious effects.

3.2. The pinned-guided compliant beam

Now considering the pinned-guided compliant beam with a tip load as shown in Fig. 3(a), the physical parameters are defined the same as those in Section 3.1, and the governing equation of the pinned-guided compliant beam can refer Eq. (2). Similarly, the boundary conditions of the pinned-guided compliant beam with a tip load can be expressed as:

$$\begin{cases} w(0,t) = 0 \\ \dfrac{\partial^2 w(0,t)}{\partial x^2} = 0 \\ \dfrac{\partial w(L,t)}{\partial x} = 0 \\ EI\dfrac{\partial^3 w(L,t)}{\partial x^3} = m_t \dfrac{\partial^2 w(L,t)}{\partial t^2} \end{cases} \tag{10}$$

Solving the governing equation for a nontrivial solution yields the following transcendental equation:

$$\frac{1}{y}\frac{2\cos y \cosh y}{\sin y \cosh y - \cos y \sinh y} = \lambda \tag{11}$$

The first three solutions of Eq. (11) are listed in Table 7 in Appendix A. We can see a similar trends as those of the fixed-guided compliant beam are obtained. That is, the value of y decreases along with the increasing of λ, and it decreases rapidly

Table 2
Parameters of the PRB model of the fixed-guided compliant beam.

Statics and kinematics		Dynamics		
Relations	Parameters	Relations	Constraints	Initial values
		$\alpha_1 = \frac{a_1}{l_1}$		
		$\alpha_2 = \frac{a_2}{l_2}$	$0 \le \alpha_1 \le 1$	
$l_1 = \frac{(1-\gamma)L}{2}$		$\alpha_3 = \frac{a_3}{l_3}$	$0 \le \alpha_2 \le 1$	$\alpha_{10} = 0.5$
$l_2 = \gamma L$	$\gamma = 0.85$	$\beta_1 = \frac{m_1}{m_b}$	$0 \le \alpha_3 \le 1$	$\alpha_{20} = 0.5$
$l_3 = l_1$	$k_\theta = 2.68$	$\beta_2 = \frac{m_2}{m_b}$	$0 \le \beta_2 \le 1$	$\beta_{10} = 0.075$
$K = 2\gamma k_\theta \frac{EI}{L}$		$\beta_3 = \frac{m_3}{m_b}$	$0 \le \beta_3 \le 1$	$\beta_{20} = 0.85$
		$\lambda = \frac{m_L}{m_b}$	$\beta_1 + \beta_2 + \beta_3 = 1$	$\beta_{30} = 0.075$
		$m_b = m_1 + m_2 + m_3$	$\lambda \ge 0$	

for $\lambda \in [0, 10]$ while gently for $\lambda \in [100,1E+6]$. y_1 continuously decreases while y_2 and y_3 converge to constant values for $\lambda \in [100,1E+6]$.

The natural frequency and normalized natural frequency of the pinned-guided compliant beam can then be calculated by Eq. (7) and Eq. (8), respectively. Validation of the continuum model of the pinned-guided compliant beam is also conducted via FEA simulations with the same parameters given in Table 1, and the results are shown in Table 8 in Appendix A. It is observed that all natural frequencies of the continuum model agree with those of the FEA simulations. Similar trends are also observed for the pinned-guided compliant beam. The larger mass ratio corresponds to the smaller natural frequency. Given the increase of the mass ratio of λ, the first modal natural frequency continuously decreases while the second and third natural frequency decrease for small λ but converge to some constant values for large λ. In addition, the lower order modal frequency may correspond to the smaller error between the continuum model and FEA model, but the mass ratio may have no effects on the errors.

4. Optimization of mass parameters of the PRB models for dynamics

In this section, we study the natural frequency of the PRB models for both of the fixed-guided and pinned-guided compliant beam.

4.1. The fixed-guided compliant beams

Non-dimensional mass property parameters are first introduced to the PRB model, then are optimized via comparing the natural frequencies of the PRB model with those of the continuum model.

4.1.1. Parametric development of the PRB model of the fixed-guided compliant beam

The PRB model of the fixed-guided compliant beam is shown in Fig. 2(b). The geometric relations of the PRB model are kept the same as those in statics and kinematics, as shown in the first column in Table 2, where l_1, l_2, and l_3 are the lengths of each segment of the PRB model, γ is the characteristic radius factor, and k_θ is the lumped stiffness of the PRB model. The parameters of γ and k_θ are original PRB parameters given in the second column in Table 2, and we keep them unchanged in order to retain the accuracy of the statics and kinematics.

In order to guarantee the natural frequency of the PRB model to be consistent with that of the continuum model, here we introduce the concept of non-dimensional mass distribution parameters β_i and α_i, from which β_i is defined as the ratio of the mass of the ith link (m_i) over the mass of the entire beam (m_b) and α_i is defined as the ratio of the distance between the mass center of the ith link and its root (a_i) over the length of the ith link (l_i). The definitions are shown the third column in Table 2. The constraints and initial values of the introduced non dimensional mass property parameters are given as shown in the fourth and fifth column in the table given the physical meaning.

The dynamics equation of the PRB model of the fixed-guided compliant beam can be obtained with the Lagrangian formulation [33], written as:

$$\boldsymbol{M}(\boldsymbol{q})\ddot{\boldsymbol{q}} + \boldsymbol{C}(\boldsymbol{q}, \dot{\boldsymbol{q}})\dot{\boldsymbol{q}} + \boldsymbol{K}\boldsymbol{q} + \boldsymbol{g}(\boldsymbol{q}) = \boldsymbol{\tau} \tag{12}$$

where $\boldsymbol{q}$ is the joint angle, $\boldsymbol{M(q)}$ is the inertia matrix, $\boldsymbol{C}(\boldsymbol{q}, \dot{\boldsymbol{q}})\dot{\boldsymbol{q}}$ represents the Coriolis force and centripetal force, $\boldsymbol{K}$ is the stiffness matrix, $\boldsymbol{g(q)}$ is the gravity term, and $\boldsymbol{\tau}$ is the motor torque. Following the derivation procedures of Lagrangian formulation, it is observed that α_1, α_3, β_1 are independent to the inertia matrix $\boldsymbol{M(q)}$. It is worth noting that $\boldsymbol{M(q)}$ includes the mass inertia and moment inertia, and both of them are calculated with respected to the rotational joint. With the dynamic formulation, the natural frequency of the PRB model may be calculated by Eq. (1) [34]. Due to the constraints of the boundary condition, the PRB model of the fixed-guided compliant beam has reduced to one degree of freedom, and only the first natural frequency can be obtained, which corresponds to the fundamental natural frequency of the continuum

model. According to Eq. (1), the fundamental natural frequency of the PRB model can be obtained as:

$$ {}^{p}f_1(\lambda) = \frac{1}{2\pi}\frac{g(\lambda, \alpha_2, \beta_2, \beta_3, \gamma, k_\theta)}{L^2}\sqrt{\frac{EI}{\rho A}} \tag{13} $$

where superscript p represents the PRB model, and $g(\lambda, \alpha_2, \beta_2, \beta_3, \gamma, k_\theta)$ is a function determined by geometric parameters for statics/kinematics and mass property parameters for dynamics, which can be expressed as follows:

$$ g(\lambda, \alpha_2, \beta_2, \beta_3, \gamma, k_\theta) = \left(\frac{4k_\theta}{\gamma}\frac{1}{\beta_2(\alpha_2^2 + \frac{1}{12}) + \beta_3 + \gamma}\right)^{\frac{1}{2}} \tag{14} $$

The normalized form of the natural frequency of the PRB model can be calculated as:

$$ {}^{p}\bar{f}_1(\lambda) = {}^{p}f_1(\lambda)\left(2\pi L^2\sqrt{\frac{\rho A}{EI}}\right) = g(\lambda, \alpha_2, \beta_2, \beta_3, \gamma, k_\theta) \tag{15} $$

4.1.2. Optimization of the PRB model of the fixed-guided compliant beam

Now we have the theoretical expression of the natural frequency for both of the continuum model and the PRB model. Next, we compare their results and optimize the non-dimensional mass parameters such that the fundamental natural frequency of the PRB model best approximates that of the continuum model. Let's define the error of the natural frequency between the PRB model and continuum model as:

$$ \bar{\delta}_1 = \left|\frac{{}^{c}\bar{f}_1 - {}^{p}\bar{f}_1}{{}^{c}\bar{f}_1}\right| \times 100\% \tag{16} $$

The ideal situation is to have the error to be 0 and one can find a relationship of the parameters of the PRB model for the fixed-guided compliant beam as:

$$ y_1^4(\lambda) = \frac{4k_\theta}{\gamma}\frac{1}{\beta_2(\alpha_2^2 + \frac{1}{12}) + \beta_3 + \gamma} \tag{17} $$

Defining the error as the objective function and the optimization problem can be formulated as:

$$ u^* = \arg\min_{u \ s.t. \ u_0} \left|\left|{}^{c}\bar{f}_1 - {}^{p}\bar{f}_1(u)\right|\right| \tag{18} $$

where $\boldsymbol{u} = (\beta_2, \beta_3, \alpha_2)$ are the optimization variables. And $\boldsymbol{u}_0$ is the boundary condition set including one equality constraint and seven inequality constraints listed in Table 2. Since the number of optimization parameters is more than number of equality constraints, there may be an infinite number of solutions or no solutions with a physical meaning. The optimized solution sets nearest to their initial condition are shown in Table 9 in Appendix A. The table compares analytical results of the continuum model, the original PRB model, and the optimized PRB model in terms of a variety of λ, in addition to the optimized dynamic parameters of the PRB model β_2, β_3, and α_2.

It is observed that the non-dimensional mass parameters can be optimized within their boundary given the mass ratio range of $\lambda \in [0, 10]$. Beyond this range, they are set to be the boundary in order to reach a minimal error. Within their boundaries, the parameter of β_2 has a trend of monotonically decreasing along with the increasing of λ while β_3 and α_2 have the trend of monotonically increasing.

It is observed that the frequency error between the original PRB model and the continuum model can be up to 6.06% at $\lambda = 0$, which may result in a significant dynamic derivation (to be discussed later). The error decreases along with the increasing of λ, which means that a light tip load may result in significant dynamic error while a heavy pay load may have small errors. However, the error can be eliminated with the optimized mass property parameters in the range of $\lambda \in [0, 10]$. Beyond this range, the parameters reach their boundary limits and cannot be optimized.

Since λ in Table 9 is discrete and finite, the optimized mass property parameters are discrete as well. To obtain a more general PRB model, we utilize an arctan function to curve fit the data in Table 9 for all mass parameters α_1, α_2, β_1, β_2, β_3 of both beam models, and they are represented by the curve fitting parameters of *a, b, c*, and *d* as given in Table 3 with 95% confidence interval.

The relation of the natural frequency verse λ is shown in Fig. 4. The stared line shows the natural frequency obtained from the continuum model, the dashed line shows the natural frequency from the original PRB model, the circled line shows the optimized PRB model with the mass parameters given in Table 9, and finally the continuous line shows the optimized PRB model with the mass parameters from curve fitting as given in Table 3. This figure shows that the original PRB model has a large deviation comparing with the continuum model in terms of the natural frequency given a small λ but have a trend of converging to the continuum model given λ of infinite large. That means, the original PRB model can be accurate given a heavy pay load with a light beam, but has larger errors for the opposite cases. However, by introducing and optimizing the mass property parameters of β_2, β_3, and α_2, the optimized PRB model can agree with the continuum model for all λ values with respect to the natural frequency. The optimized PRB model with the curve fitted mass property parameters can pass through all discrete points of the continuum model, hence may be used for accurately modeling of the dynamics of the compliant beam with a continuous range of λ.

Table 3
The complete table of the PRB model.

	Kinematics & statics parameters	Parameters for dynamics of PRB model				
		Original PRB model	Optimized PRB model $a\arctan(b\lambda + c) + d$			
				a	b	c	d
Fixed-guided compliant beam	$\gamma = 0.85$ $k_\theta = 2.68$	$\beta_{20} = 0.85$ $\beta_{30} = 0.075$ $\alpha_{20} = 0.5$	$\beta_2(\lambda)$	−0.2789	2.178	−5.584	0.4111
			$\beta_3(\lambda)$	0.3026	2.377	−6.163	0.5518
			$\alpha_2(\lambda)$	0.153	3.218	−5.536	0.7681
Pinned-guided compliant beam		$\beta_{10} = 0.85$ $\beta_{20} = 0.15$ $\alpha_{10} = 0.5$	$\beta_1(\lambda)$	−0.2699	2.219	−5.82	0.3979
			$\beta_2(\lambda)$	0.2699	2.222	−5.826	0.6021
			$\alpha_1(\lambda)$	0.1444	3.125	−3.882	0.7817

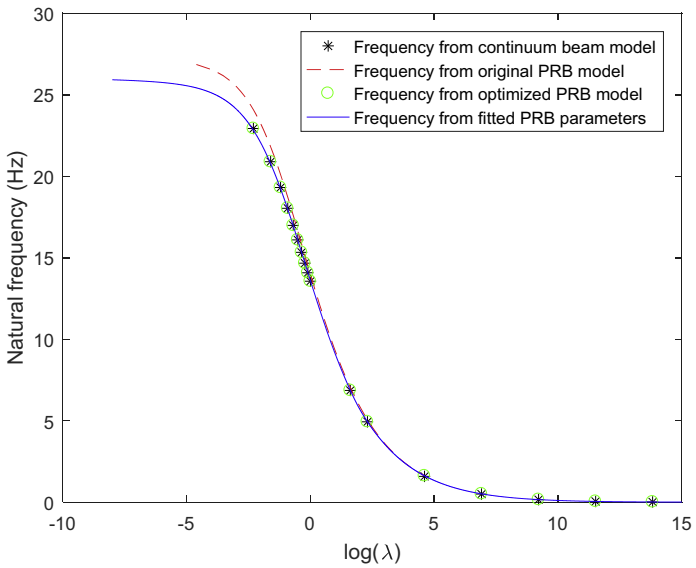

Fig. 4. Natural frequency vs. mass ratio of the fixed-guided beam.

Table 4
Parameters of the PRB model of the pinned-guided compliant beam.

Statics and kinematics		Dynamics		
Relations	Parameters	Relations	Constraints	Initial values
$l_1 = \gamma L$	$\gamma = 0.85$	$\alpha_1 = \frac{a_1}{l_1}$	$0 \le \alpha_1 \le 1$	$\alpha_{10} = 0.5$
$l_2 = (1-\gamma)L$	$k_\theta = 2.68$	$\alpha_2 = \frac{a_2}{l_2}$	$0 \le \alpha_2 \le 1$	$\alpha_{20} = 0.5$
$K = \gamma k_\theta \frac{EI}{L}$		$\beta_1 = \frac{m_1}{m_b}$	$0 \le \beta_1 \le 1$	$\beta_{10} = 0.85$
		$\beta_2 = \frac{m_2}{m_b}$	$0 \le \beta_2 \le 1$	$\beta_{20} = 0.15$
		$\lambda = \frac{m_t}{m_b}$	$\beta_1 + \beta_2 = 1$	
		$m_b = m_1 + m_2$	$\lambda \ge 0$	

4.2. The pinned-guided compliant beam

In this section, we will follow a similar procedure to obtain the optimized PRB model for the pinned-guided compliant beams.

4.2.1. Parametric development of the PRB model of the pinned-guided compliant beam

The parameterized PRB model is shown in Fig. 3(b). The geometric parameter of the statics and kinematics plus the introduced mass property parameters of the PRB model are given in Table 4. The characteristic radius factor γ and stiffness coefficient k_θ are kept unchanged as shown in the table. The constraints and initial values of the mass property parameters are shown in the table as well.

The dynamic equations can be derived with the Lagrangian method and have the form of Eq. (12). Again, the inertia matrix is independent of α_2. Following the same procedure as Section 4.1.1, we can obtain the natural frequency and the

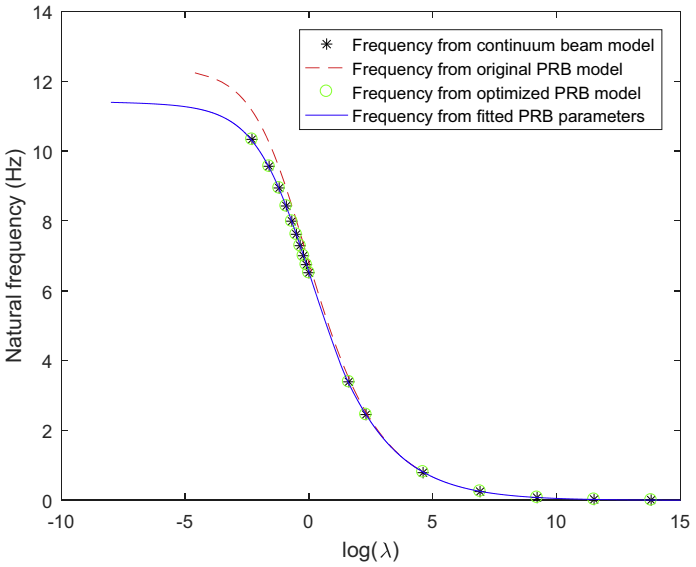

Fig. 5. Natural frequency vs. mass ratio of the pinned-guided beam.

normalized natural frequency of the PRB model of the pinned-guided compliant beam as:

$$ {}^{p}f_1(\lambda) = \frac{1}{2\pi}\frac{h(\lambda,\alpha_1,\beta_1,\beta_2,\gamma,k_\theta)}{L^2}\sqrt{\frac{EI}{\rho A}} \tag{19} $$

$$ {}^{p}\bar{f}_1(\lambda) = h(\lambda,\alpha_1,\beta_1,\beta_2,\gamma,k_\theta) \tag{20} $$

where $h(\lambda, \alpha_1, \beta_1, \beta_2, \gamma, k_\theta)$ is a function determined by the parameters associated with statics, kinematics, and dynamics of the PRB model, and can be expressed as follows:

$$ h(\lambda,\alpha_1,\beta_1,\beta_2,\gamma,k_\theta) = \left(\frac{k_\theta}{\gamma}\frac{1}{\beta_1(\alpha_1^2+\frac{1}{12})+\beta_2+\gamma}\right)^{\frac{1}{2}} \tag{21} $$

4.2.2. Optimization of the PRB model of the pinned-guided compliant beam

With the theoretical expressions of the natural frequency of the continuum model and PRB model of the pinned-guided compliant beam, one can also obtain the relationship of the mass property parameters of the pinned-guided compliant beam as:

$$ y_1^4(\lambda) = \frac{k_\theta}{\gamma}\frac{1}{\beta_1(\alpha_1^2+\frac{1}{12})+\beta_2+\gamma} \tag{22} $$

Similar to the case of the fixed-guided compliant beam, we can also formulate this problem into a parameter optimization problem as in Eq. (18) with $u = (\beta_1, \beta_2, \alpha_1)$ being the optimization variables. The results for various λ are shown in Table 10 in Appendix A. It shows that the mass property parameters may start from their initial value and converge to their boundary conditions. Within their boundaries, the parameter of β_1 has a trend of monotonically decreasing along with the increasing of λ while β_2 and α_1 have the trend of monotonically increasing. Fig. 5 shows that the optimized PRB model can accurately predict the natural frequency of the continuum model. The maximum error is up to 9.32% at $\lambda = 0$.

5. Performance evaluation of the dynamics of the PRB models

After the derivation of the parameterized PRB models, we will apply the developed PRB models of the compliant beams to compliant mechanisms and evaluate their dynamic performance via comparing with FEA simulations in this section. It is worth noting that the NLgeom is turned on in Abaqus for considering large deflection effects or large strain effects.

5.1. The fixed-root compliant parallel-guiding mechanism

According to Fig. 4, the error between the original PRB models and continuum model is relatively large for small λ and decreases along with the increasing of λ. It may be not necessary to test all cases of λ to validate the dynamics. Instead,

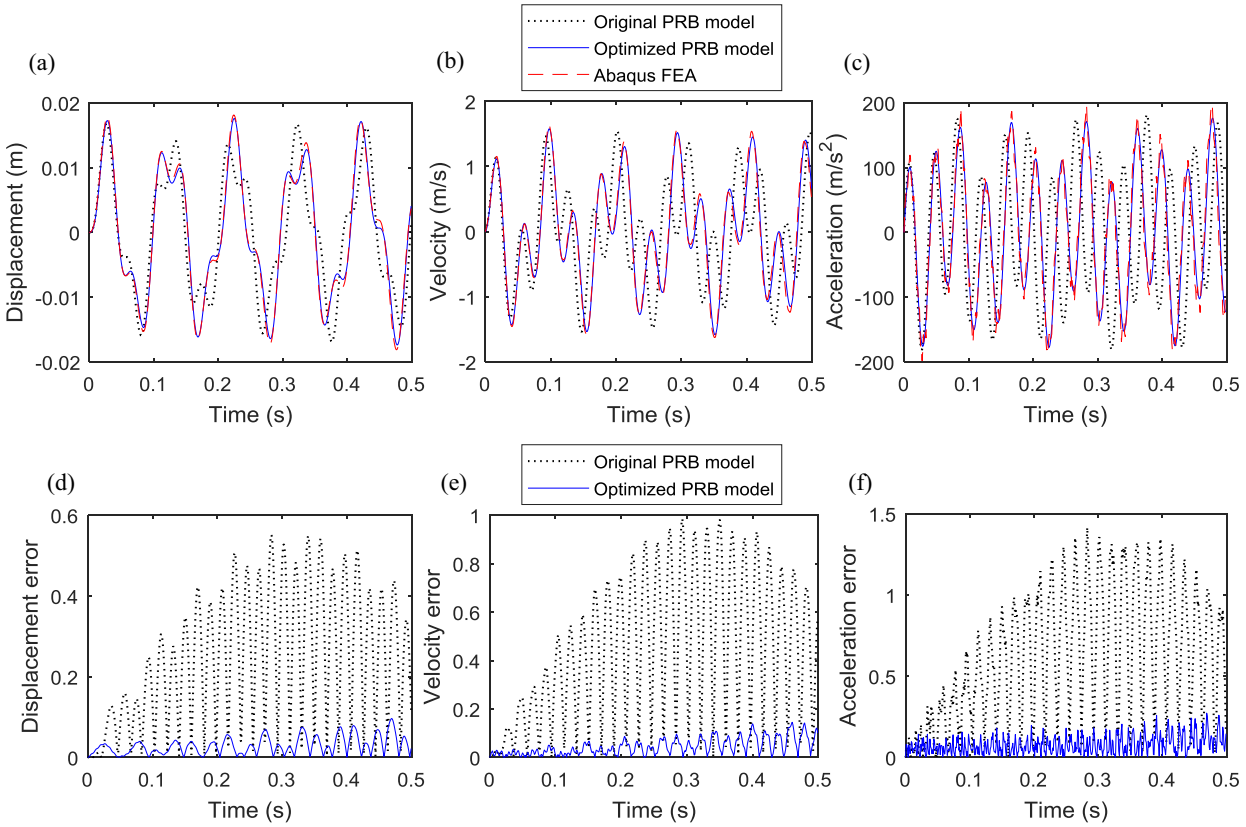

Fig. 6. Evaluations of the dynamics of the PRB models for the fixed-root compliant parallel-guiding mechanism given the sinusoidal force with $A = 10$ N, $\omega = 10$ Hz, and $\lambda = 0$. (a) displacement response, (b) velocity response, (c) acceleration response, (d) error of displacement response, (e) error of velocity response, (f) error of acceleration response.

we pick a few typical λ such as $\lambda_1 = 0$, $\lambda_2 = 0.5$, and $\lambda_3 = 10$ for dynamics validation. In terms of the fixed-guided compliant beam, we have studied its fundamental natural frequency with analytical expressions of the original PRB model, the optimized PRB model, and the continuum model, plus the fundamental frequency of its FEA model. The simulation models of the fixed-root CPGM based on the fixed-guided compliant beam are built in existing commercial software. More specifically, the original and optimized PRB models were built in ADAMS while the compliant FEA model was built in Abaqus. The original/optimized PRB model of the fixed-root CPGM is comprised of two sets of the original/optimized PRB model of the fixed-guided compliant beam, according to the discussion in Section 2. The parameters of the original PRB model, the optimized PRB model, and the FEA model of the fixed-root CPGM are from the fixed-guided beam model.

Prior to conducting the dynamic analysis, we first do a quick check of the fundamental frequency of all models. The natural frequency can be obtained from the analytical models, from frequency analysis in FEA simulations (Abaqus), or from Fast Fourier Transform (FFT) of the response of multi-body dynamics simulations (ADAMS). And their results are shown in Table 11 in Appendix A.

The results show that natural frequency of the original PRB model, the optimized PRB model, and the Abaqus FEA model of the fixed-root CPGM agree with that of the fixed-guided compliant beam. However, the natural frequency of the original PRB model has a deviation from that of the FEA model. This table has shown that the optimized PRB model developed from the fixed-guided compliant beam can be used for the fixed-root CPGM. Next, we will check if the dynamics of the optimized PRB model can agree with that of the FEA model for the case of the fixed-root CPGM.

Here sinusoidal signals as the input force are applied at the tip of the fixed-root CPGM, and we check the output performance such as displacement, velocity, and acceleration at the stage. The Abaqus FEA simulation, which is a continuum beam, is assumed to be the reference, and the ADAMS simulation, which contains both of the original PRB model and optimized PRB model, are those to be evaluated.

Assume the applied input force in terms of time t is in the sinusoidal form of $F = A\sin(2\pi\omega t)$, where A is the magnitude, ω is the input frequency. Given $\lambda = 0$, $A = 10$ N and $\omega = 10$ Hz, the time response is shown in Fig. 6. Fig. 6(a)–(c) show the time response of the displacement, velocity, and acceleration, respectively, from which the dotted line is the original PRB response, the continuous line is the optimized PRB response, and the dashed line is the FEA response. Fig. 6(d)–(f) show the corresponding errors between the PRB models and the FEA model, from which the dotted line shows the output error between the original PRB model and the FEA model while the continuous line shows the error between the optimized PRB

model and the FEA model. The dynamics error is defined as:

$$\epsilon(t) = \frac{|^c z(t) - {}^p z(t)|}{\max(^c z(t))} \tag{23}$$

where $z(t)$ may be displacement, velocity, or acceleration, the superscript c represents the continuum FEA model, and the superscript p represents the PRB model (either original or optimized). The figure shows that, in addition to the displacement, the velocity and acceleration of the optimized PRB model agree with those of the FEA model as well, but the original PRB model has larger deviations. The figure also shows that the error of the original PRB model is significantly larger than that of the optimized PRB model.

Here we define a parameter ξ for deformation of beam length:

$$\xi = \frac{\Delta}{L} \times 100\% \tag{24}$$

where Δ is the tip deflection and L is the length of the CPGM. The figure shows that ξ is up to 8%. It is also observed that the displacement error is less than velocity error, and the velocity error is less than the acceleration error. Furthermore, it shows that the error of the displacement is smooth while it has many sharp oscillations from the error of the acceleration. Finally, the simulation shows that the PRB model is significantly efficient than the FEA simulation. Given the same simulation steps of 1000 in Abaqus and ADAMS, the Abaqus FEA runs around 2 h to complete the dynamics simulation while the PRB models in ADAMS requires less than 1 min (Hardware: Intel ® Xeon ® CPU E7- 4870 2.4 Ghz 8 Cores). Overall, the simulation demonstrates that the optimized PRB model developed in Section 4 can accurately and efficiently predict the dynamics of the fixed-root CPGM given the input force. As we discussed in Section 4, the possible maximum error occurs at $\lambda = 0$. Since the optimized PRB model can precisely model the dynamics of the fixed-root CPGM at $\lambda = 0$, we expect that the larger λ will work even better, which will be shown later.

Next, we study how the magnitude of the input force of A, the frequency of the input force of ω, and the mass ratio of λ affect the accuracy of the optimized PRB model.

5.1.1. Effects of the input magnitude

We have validated that the optimized PRB model is accurate for the case of $A = 10$ N, $\omega = 10$ Hz, and $\lambda = 0$ with $\xi = 8\%$. Here we would like to increase the magnitude of the input force while retaining the input frequency as $\omega = 10$ Hz and $\lambda = 0$ and to explore how large the magnitude can be and how it affects the accuracy. We gradually increase the magnitude up to $A = 100$ N, and the optimized PRB model can still basically follows the FEA model given $\xi = 44.31\%$. It turns out that the magnitude of the deformation monotonically increases with the increasing of the magnitude of the input force. Larger input force magnitudes result in large errors.

5.1.2. Effects of the input signal frequency

Now, let us take a look at effects of the input signal frequency ω. Intuitively, the PRB model (both the original and optimized one) is accurate to model the low frequency dynamics (which is close to the static cases). On the other hand, the PRB models may not be accurate for dynamics of high input frequency, since it may excite high modal natural frequencies but both PRB models only have 1 DOF with 1 modal natural frequency.

To study the effects of different input frequencies on the dynamic performance of the fixed-root CPGM, we select the input signal frequency based on the natural frequencies of the fixed-root CPGM. More specifically, the input frequencies are chosen between two adjacent natural frequencies of the fixed-root CPGM. For the cases of $\lambda_1 = 0$, $\lambda_2 = 0.5$, and $\lambda_3 = 10$, the first three natural frequencies of the fixed-root CPGM can refer from Table 6.

Taking $\lambda = 0$ as an example, the first three natural frequencies are 25.735 Hz, 139.13 Hz, and 343.99 Hz, respectively. Here we explore the input frequency of 10 Hz, 100 Hz, and 200 Hz while keeping $\lambda = 0$ and $A = 10$ N. Fig. 7 shows the displacement response given the input force with different input frequencies of 10 Hz, 100 Hz, and 200 Hz. Given the input frequency of $\omega = 10$ Hz, the optimized PRB can follow the FEA output very well but the original PRB has large deviations. Neither PRB models can follow the FEA model at $\omega = 100$ Hz. However the optimized PRB model performs better than the original PRB model. The same conclusion can be drawn for $\omega = 200$ Hz. In terms of the frequency error, the original PRB model has larger error than that of the optimized PRB for all of three cases, and the difference of the errors are significantly large at the low frequency of $\omega = 10$ Hz while slightly large at the high frequencies of $\omega = 100$ Hz and $\omega = 200$ Hz. That means, the optimized PRB model performs significantly better than the original PRB model at low input frequencies, but their performances are close at high input frequencies. This figure also shows that the optimized PRB model may work well given the input force with a frequency below or around its fundamental frequency, and may lose the accuracy if the input signal frequency is very high.

5.1.3. Effects of the mass ratio

Next, we study effects of the mass ratio λ on the dynamic performance. Given the same input of $A = 10$ N and $\omega = 200$ Hz but with different mass ratios of 0, 0.5, and 10, the displacement response is shown in Fig. 8. The figure shows that the original and optimized PRB model have a close performance given $\omega = 200$ Hz, which do not agree with the FEA model at λ =0, but both of them track the model well at λ =10. It is clear to see that a larger λ results in a smaller error for both

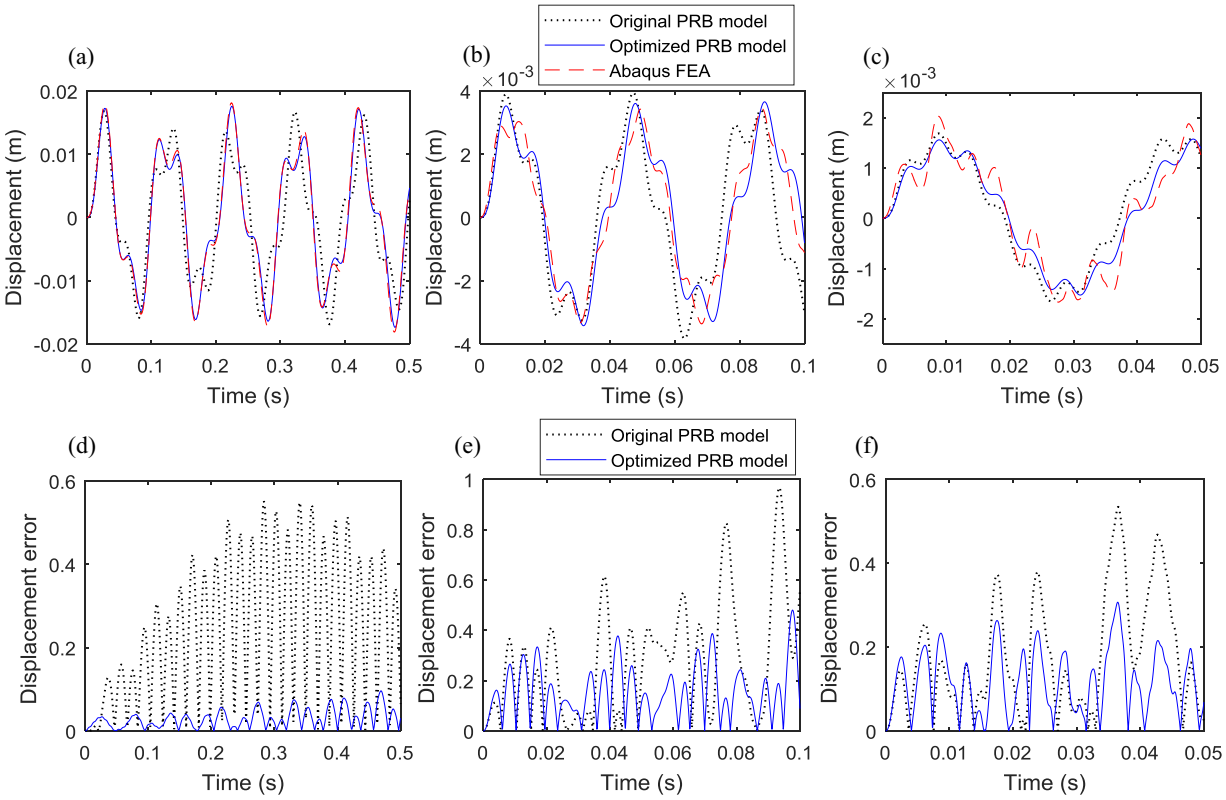

Fig. 7. Exploration of the effect of the input frequency on the output response for the fixed-root parallel-guiding mechanism. (a) and (d) are given the input of $A = 10$ N, $\omega = 10$ Hz, and $\lambda = 0$, (b) and (e) are given the input of $A = 10$ N, $\omega = 100$ Hz, and $\lambda = 0$, (c) and (f) are given the input of $A = 10$, $\omega = 200$ Hz, and $\lambda = 0$.

PRB models, which agrees with the discussion in Section 4. The PRB models are not accurate given $\lambda = 0$ with $A = 10$ N and $\omega = 200$ Hz, but they can be precise if λ increases from 0 to 10. This figure also shows that the optimized and original PRB model do not have a significant difference at the input frequency of $\omega = 200$ Hz for the case of the pinned-root CPGM, either both inaccurate for small λ or both precise for large λ.

5.1.4. The frequency domain analysis

To further understand the dynamic response of the fixed-root CPGM, FFTs of the time response signals are conducted in order to analyze the data in the frequency domain. Fig. 9 shows the frequency response given $A = 10$ N, $\omega = 200$ Hz, and $\lambda = 0$ for the fixed-root CPGM. The figure shows the magnitude and phase and their errors of the displacement, velocity, and acceleration.

According to the magnitude and phase plot of the displacement in Fig. 9(a) and (b), it is clear to see that the output response of both PRB models contains two frequencies, one of which is their natural frequency (25.5 Hz for the optimized PRB model and 27.1 Hz for the original PRB model) and the other is the input frequency (200 Hz). However, the FEA response has four signals including the first three natural frequencies which are 25.7 Hz, 138.7 Hz and 342.43 Hz as given in Table 6, plus the input frequency of 200 Hz. As shown in Fig. 9(d) and (e), the optimized PRB model agrees with the FEA model well at the fundamental frequency while the original PRB model cannot. However, both of the PRB models cannot track the second and third natural frequency of the FEA model since both of the PRB models have a single DOF with a single modal natural frequency. Furthermore, it shows that the fundamental natural frequency may be excited as a dominated response since its magnitude is significantly larger than those of the high modal natural frequencies. Finally, this figure shows that the optimized PRB model can still track the FEA model well at its fundamental frequency (25.7 Hz) in terms of the displacement response, and the error shown in the time domain of Fig. 8(a) and (d) comes from the excitations of the high modal natural frequencies of the FEA model.

Now let's take a look at the velocity response of Fig. 9(c) and (g). It is observed that the fourth modal natural frequency around 625 Hz of the fixed-root CPGM is excited as well, which is not observable in the displacement response. It may result from the tiny magnitude of the displacement response exited by the fourth modal natural frequency. It well explains that the velocity response in the time domain has more fluctuation and less smooth than that of the displacement response as shown in Fig. 6, since it contains a wider frequency spectrum than that of the displacement response. The figure also shows

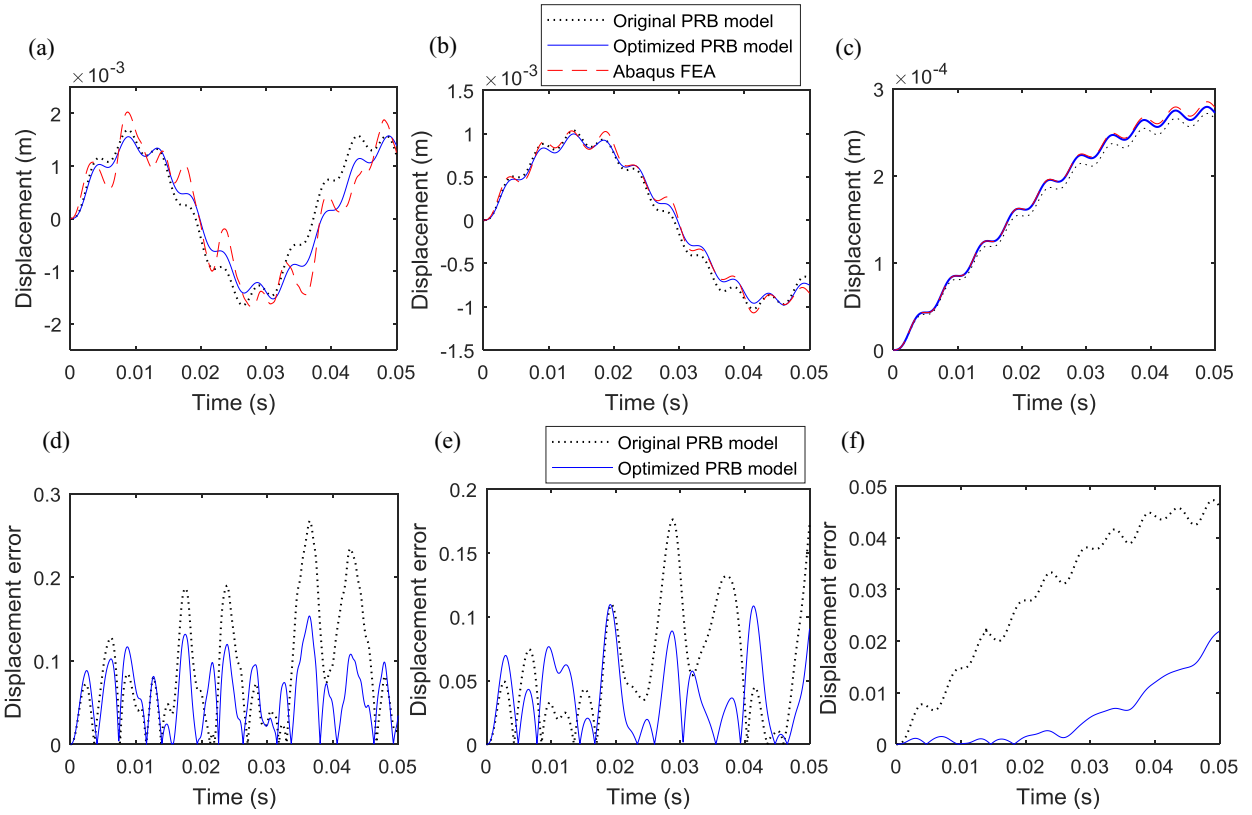

Fig. 8. Exploration of the effect of the mass ratio on the output response for the fixed-root compliant parallel-guiding mechanism. (a) and (d) are given the input of $A = 10$ N, $\omega = 200$ Hz, and $\lambda = 0$, (b) and (e) are given the input of $A = 10$ N, $\omega = 200$ Hz, and $\lambda = 0.5$, (c) and (f) are given the input of $A = 10$, $\omega = 200$ Hz, and $\lambda = 10$.

that the optimized PRB model follows the FEA model well at its fundamental frequency (25.7 Hz) in terms of the velocity and the error in the time domain comes from the excitations of the high modal natural frequencies of the FEA model.

The acceleration response of Fig. 9(h) and (i) show that an even higher order natural frequency around 910 Hz is excited as well and it is not observable from the frequency response of the displacement and velocity. It well explains that the acceleration response in the time domain has the highest fluctuation and the least smooth among the responses of displacement, velocity, and acceleration as shown in Fig. 6 due to its widest frequency spectrum. The figure also shows that the optimized PRB model can track the FEA model well at its fundamental frequency (25.7 Hz) in terms of the acceleration, and the error in the time domain comes from the excitations of the high modal natural frequencies of the FEA model.

We have studied the frequency domain with extensive cases of A, ω, and λ, and some of them are given in the supplemental material. It turns out that the input frequency significantly affects the frequency domain response and the accuracy of the optimized PRB model for the fixed-root CPGM. Given a low input frequency (close or less than the fundamental natural frequency), the fundamental natural frequency is excited and dominates the response, from which the optimized PRB model can accurately and effectively predict the dynamics of the fixed-root CPGM. However, a larger input frequency will excite high modal natural frequencies in addition to the low modal ones, from which the optimized PRB model gradually lose its accuracy since it can only track the fundamental natural frequency but can do nothing on high modal natural frequencies.

5.2. The pinned-root compliant parallel-guiding mechanism

In this section, we evaluate the optimized PRB model for the pinned-root CPGM. The mass ratios of $\lambda = 0$, $\lambda = 0.5$, and $\lambda = 10$ are the typical values studied here. In terms of the pinned-guided compliant beam, we have studied the fundamental natural frequency with analytical expressions of the original PRB model, the optimized PRB model, and the continuum model, plus the fundamental frequency of its FEA model. Here we build the simulation models of the pinned-root CPGM based on the pinned-guided compliant beam. Similar to the case of the fixed-root CPGM, the original/optimized PRB model of the pinned-root CPGM is built in ADAMS comprised of two sets of the original/optimized PRB model of the pinned-guided compliant beam. The parameters of the original PRB model, the optimized PRB model, and the FEA model of the fixed-root CPGM are directly from the fixed-guided compliant beam.

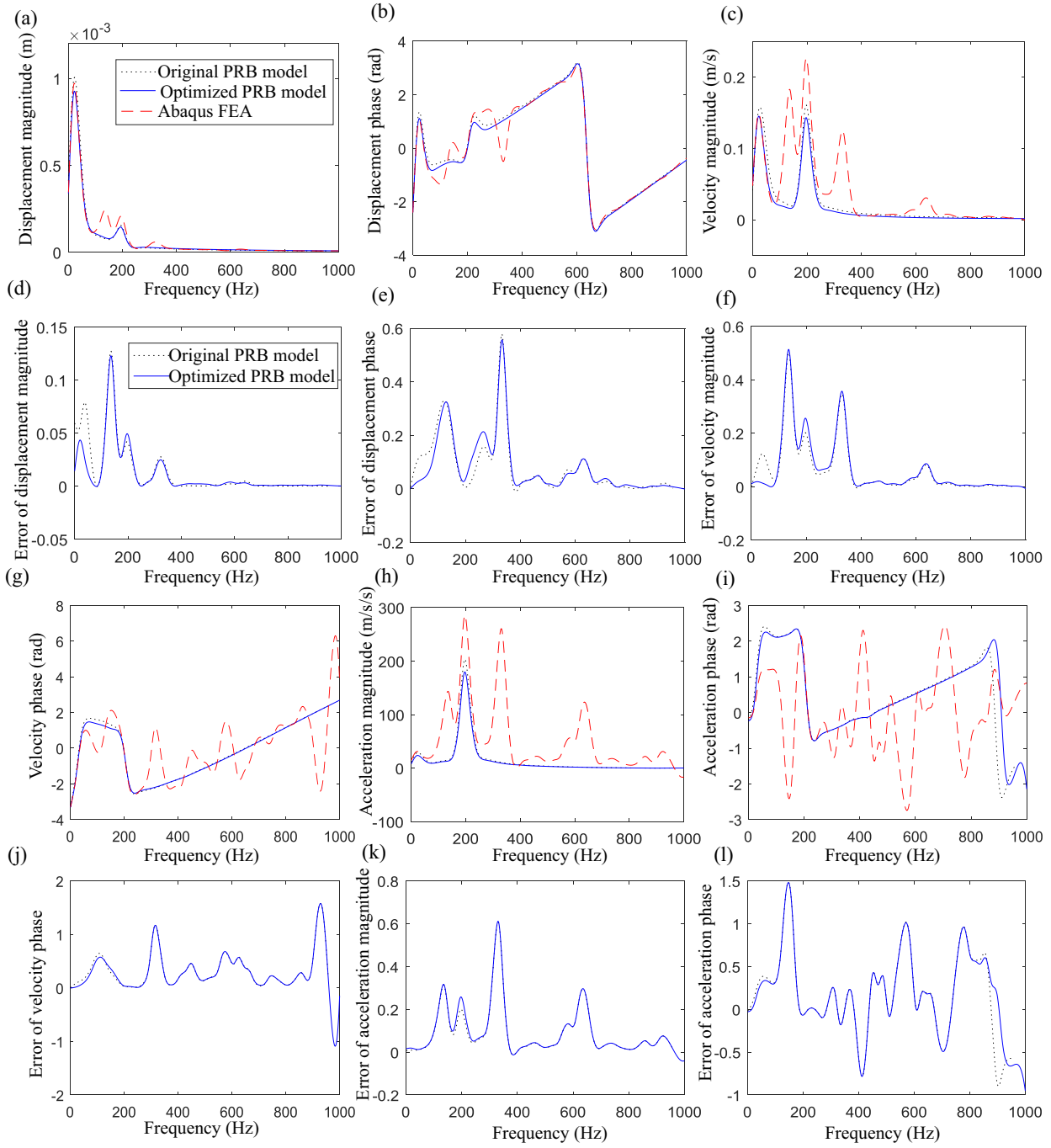

Fig. 9. The frequency domain analysis of the response of the fixed-root compliant parallel-guiding mechanism at $A = 10$ N, $\omega = 200$ Hz, and $\lambda = 0$. (a) and (d) represent the magnitude of the displacement and the associated error, (b) and (e) represent the phase of the displacement and the associated error, (c) and (i) represent the magnitude of the velocity and the associated error, (g) and (j) represent the phase of the velocity and the associated error, (h) and (k) represent the magnitude of the acceleration and the associated error, (i) and (l) represent the phase of the acceleration and the associated error.

Before we conduct the dynamics simulation, we did a quick check of the natural frequency of those models with the results shown in Table 12 in Appendix A. The results show that the natural frequency of the original PRB model, the optimized PRB model, and the Abaqus FEA model of the pinned-guided compliant beam agree with that of the pinned-root CPGM, as we discussed in Section 2. The optimized PRB model is consistent with the FEA model for the pinned-root CPGM in terms of the fundamental natural frequency, while the original PRB model has a deviation from that of the FEA model. This table shows that the optimized PRB model of the pinned-guided compliant beam can be used for the pinned-root CPGM.

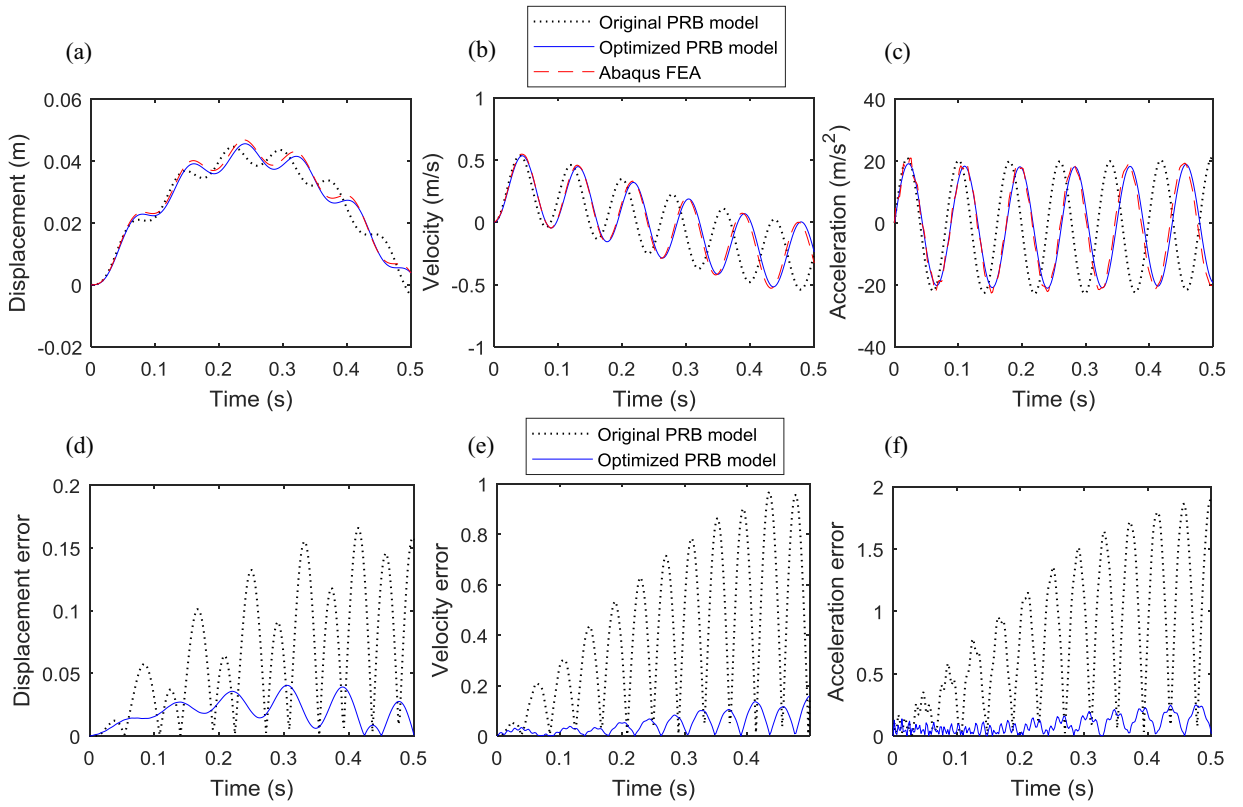

Fig. 10. Evaluations of the dynamics of the PRB model for the pinned-root compliant parallel-guiding mechanism given $A = 10$ N, $\omega = 1$ Hz, and $\lambda = 0$. (a) displacement response, (b) velocity response, (c) acceleration response, (d) error of displacement response, (e) error of velocity response, (f) error of acceleration response.

In subsections below, we will follow a similar procedure as the case of fixed-root CPGM to assess effects the magnitude of the force of A, the input frequency of ω, and the mass ratio of λ on the accuracy of dynamics performance.

5.2.1. Effects of the input magnitude

The fundamental natural frequency of the pinned-root CPGM is 11.39 Hz, and we first study the response given a low input frequency of $\omega = 1$ Hz. Given $A = 10$ N, $\omega = 1$ Hz, and $\lambda = 0$, the deformation is up to $\xi = 20\%$ as shown in Fig. 10. Fig. 10(a)–(c) show the response of the displacement, velocity, and acceleration of the pinned-root CPGM, and Fig. 10(d)–(f) show the corresponding errors between the PRB models and the FEA model. Similar conclusions as those in Section 5.1.1 are obtained. The figure shows that the optimized PRB model agrees with the FEA model, but the original PRB model has large deviations.

It turns out that the magnitude of the deformation monotonically increases with the increasing of the magnitude of the input force.

5.2.2. Effects of the input frequency

Similar to the case of the fixed-root CPGM, we would like to explore the effects of the input frequency ω on the output response. The first three natural frequencies of the pinned-root CPGM at $\lambda = 0$ are 11.352 Hz, 102.31 Hz, and 284.6 Hz. Here we pick three input frequencies of 1 Hz, 50 Hz, and 200 Hz while holding $\lambda = 0$ and $A = 10$ N unchanged. Fig. 11 shows the displacement response given the input force with different frequencies of 1 Hz, 50 Hz, and 200 Hz. Given the input frequencies ω of 1 Hz and 50 Hz, the optimized PRB model can follow the FEA output very well but the original PRB model has deviations. At $\omega = 200$ Hz, both of the original and the optimized PRB model cannot follow the FEA response. We observed similar trends as those in Section 5.1.2. The error of the optimized PRB model increases along with the increasing of the input frequency.

5.2.3. Effects of the mass ratio

We also study the effect of the mass ratio on the output response for the pinned-root CPGM. Given the same input of $A = 10$ N and $\omega = 200$ Hz but with different mass ratios of λ of 0, 0.5, and 10, the displacement output is shown in Fig. 12. The figure shows that the optimized PRB model performs close to the original PRB model, and both of them cannot track

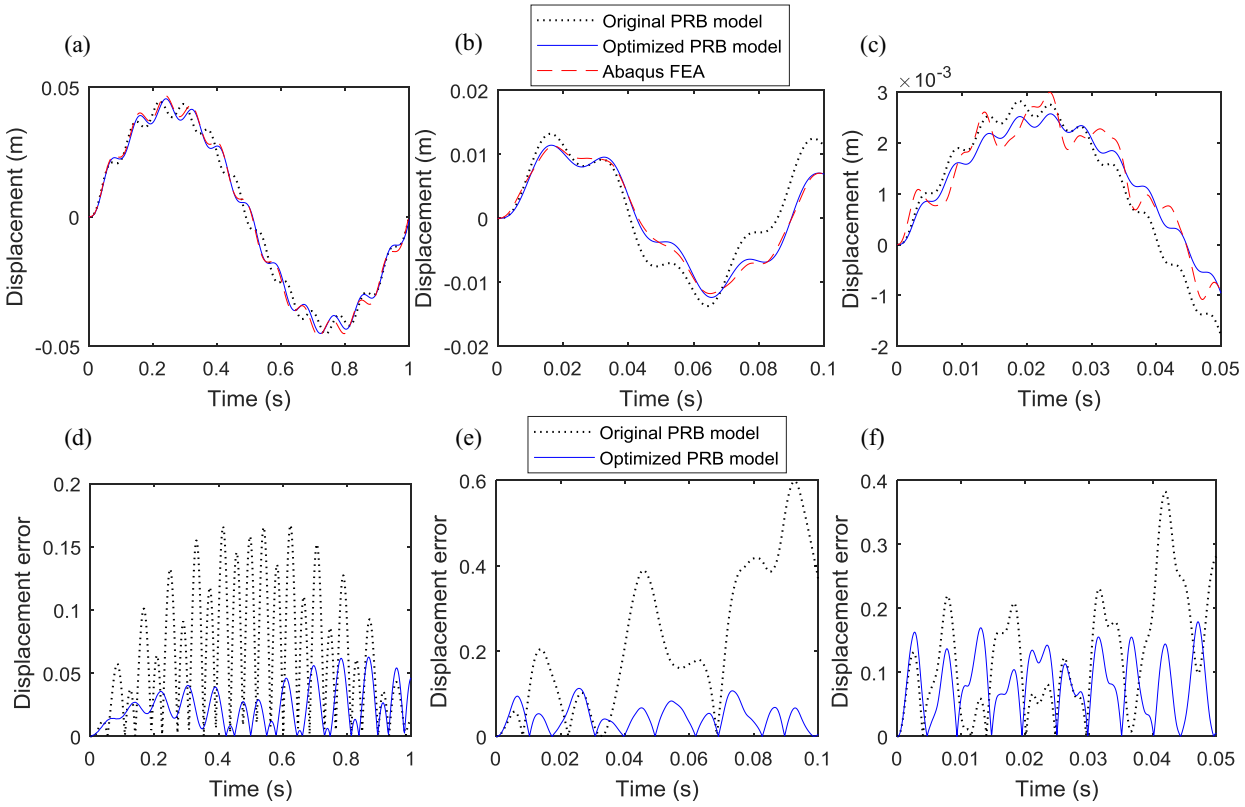

Fig. 11. Exploration of the effect of the input frequency on the output response for the pinned-root parallelogram mechanism. (a) and (d) are given the input of $A = 10$ N, $\omega = 1$ Hz, and $\lambda = 0$, (b) and (e) are given the input of $A = 10$ N, $\omega = 50$ Hz, and $\lambda = 0$, (c) and (f) are given the input of $A = 10$, $\omega = 200$ Hz, and $\lambda = 0$.

the FEA model at $\lambda = 0$. Both of the PRB modes perform better at $\lambda = 0.5$ than that at $\lambda = 0$ but still have some derivations. However, they can track the FEA model very well with very small errors at $\lambda = 10$. Similar conclusions are drawn as those in Section 5.1.3. The larger λ can result in the smaller error for both PRB models.

5.2.4. The frequency domain analysis

Fig. 13 shows the magnitude and phase plot and their errors with respect to displacement, velocity, and acceleration by using the frequency domain analysis for the case $A = 10$ N, $\omega = 200$ Hz, $\lambda = 0$.

According to the magnitude and phase plot of the displacement in Fig. 13(a) and (b), it is clear to see that the output response of both of the PRB models only contain two frequencies, from which one is the natural frequency (11.383 Hz for the optimized PRB model and 12.421 Hz for the original PRB model) and another is the input frequency of 200 Hz. However, the FEA response has four signals including the first three natural frequencies which are 11.352 Hz, 102.31 Hz, and 284.6 Hz as given in Table 8, plus the input frequency of 200 Hz.

According to the magnitude and phase error given in Fig. 13(d) and (e), the optimized PRB model can track the FEA model well at the fundamental frequency but the original PRB model cannot. It has a smaller error comparing with the original PRB model. However, both of the PRB models cannot track the second and third natural frequency of the FEA model since both of them have a single DOF. Furthermore, it shows that the first natural frequency may be excited as a dominated response since its magnitude is significantly larger than those of the higher modal natural frequencies. Finally, this figure shows that the optimized PRB model can track the FEA model well at its fundamental frequency (11.38 Hz) in terms of displacement, and the error shown in the time domain of Fig. 12(a) and (d) comes from the excitations of the high modal natural frequencies of the FEA model.

Considering the velocity response of Fig. 13(c) and (g), it is observed that the fourth and fifth modal natural frequency around 570 Hz and 910 Hz are also excited with a small magnitude, which is not observable in the displacement response. It well explains that the velocity response in the time domain has more fluctuation and less smooth than that of the displacement response as shown in Fig. 10 since it contains a wider frequency spectrum. The figure also shows that the optimized PRB model can track the FEA model well at its fundamental frequency (11.38 Hz) in terms of the velocity and the error in the time domain comes from the excitations of the high modal natural frequencies of the FEA model.

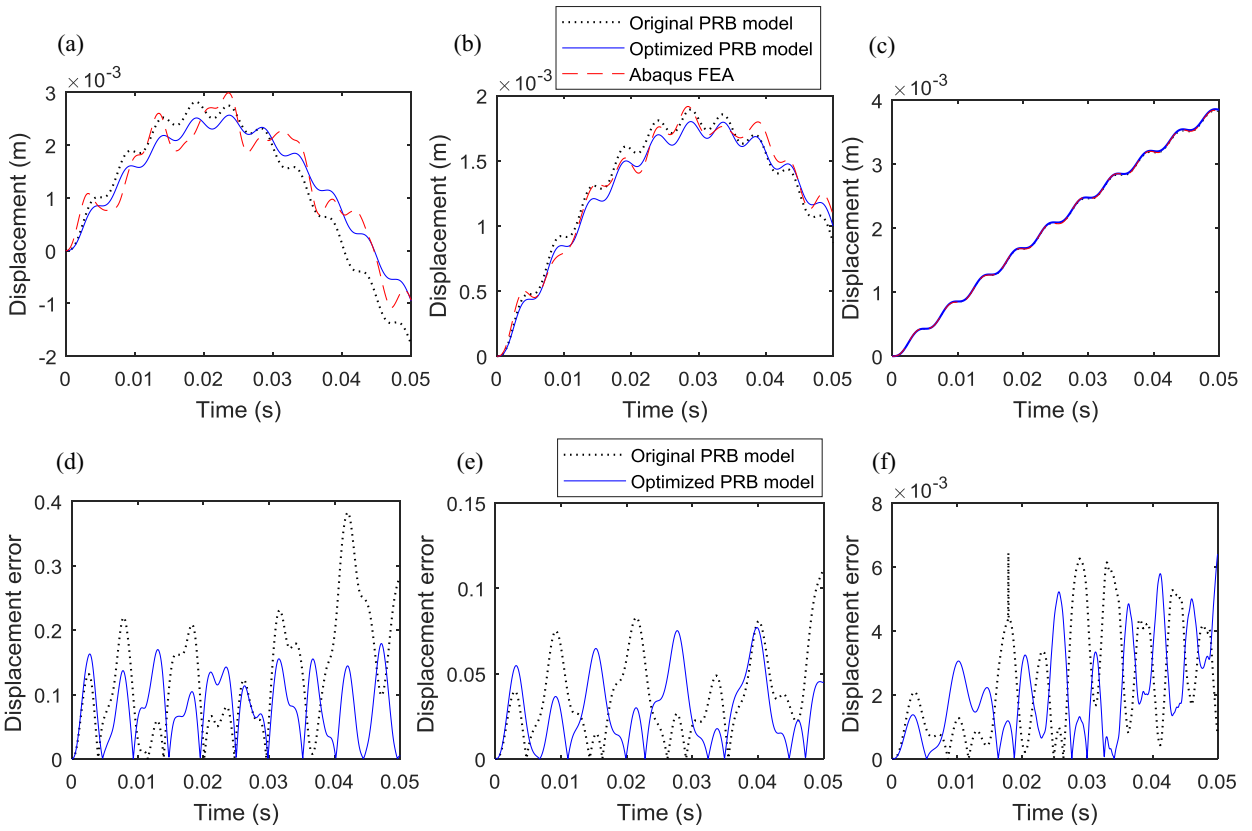

Fig. 12. Effects of mass ratio and input frequency on output response of the pinned-root compliant parallel-guiding mechanism. (a) and (d) are given the input of $A = 10$ N, $\omega = 200$ Hz, and $\lambda = 0$, (b) and (e) are given the input of $A = 10$ N, $\omega = 200$ Hz, and $\lambda = 0.5$, (c) and (f) are given the input of $A = 10$, $\omega = 200$ Hz, and $\lambda = 10$.

The acceleration response of Fig. 13(h) and (i) show a slightly large excitation of the magnitude of the fourth and fifth modal natural frequency. It well explains that the acceleration response in the time domain has the highest fluctuation and the least smooth among the displacement, velocity, and acceleration response, as shown in Fig. 10. The figure also shows that the optimized PRB model can track the FEA model well at its fundamental natural frequency (11.38 Hz) in terms of the acceleration, and the error in the time domain comes from the excitations of the high modal natural frequencies of the FEA model.

We also studied the frequency domain on a variety values of A, ω, and λ, from which some of them are shown in the supplemental material. It turns out that the input frequency significantly affects the frequency domain for the case of the pinned-root CPGM. Similar conclusions are made as those in Section 5.1.4. The optimized PRB model can track the FEA model very well at low input frequencies but lose the accuracy at high input frequencies.

6. Discussions and conclusions

This paper presents the framework of optimizing the original PRB model to predict the dynamics of compliant mechanisms, and the continuum model is used as a reference for the original PRB model in terms of the natural frequency. In this study, the linear continuum model is used as the reference for convenient analysis. For the applications requiring high accuracy with large deformations, a nonlinear continuum model working for large deformations is suggested as the reference for the optimization procedure.

This paper develops optimized PRB models that can accurately predict statics, kinematics, and dynamics for compliant mechanisms by introducing non-dimensional mass property parameters. Two typical mechanisms: fixed-root and pinned-root compliant parallel guided mechanisms, were employed as case studies. We show that the fundamental natural frequency of the optimized PRB model well agrees with that of the continuum model, and the dynamics of the optimized PRB model is consistent with that of the continuum model at low input signal frequencies. The results show that the accuracy of the optimized PRB model is significantly improved comparing with that of the original PRB model, given a variety of mass ratios and input frequencies/amplitudes. We also studied the effect of the mass ratio and input magnitude/frequency on the dynamic accuracy. The proposed optimized PRB model has significantly reduced the computation load while retaining

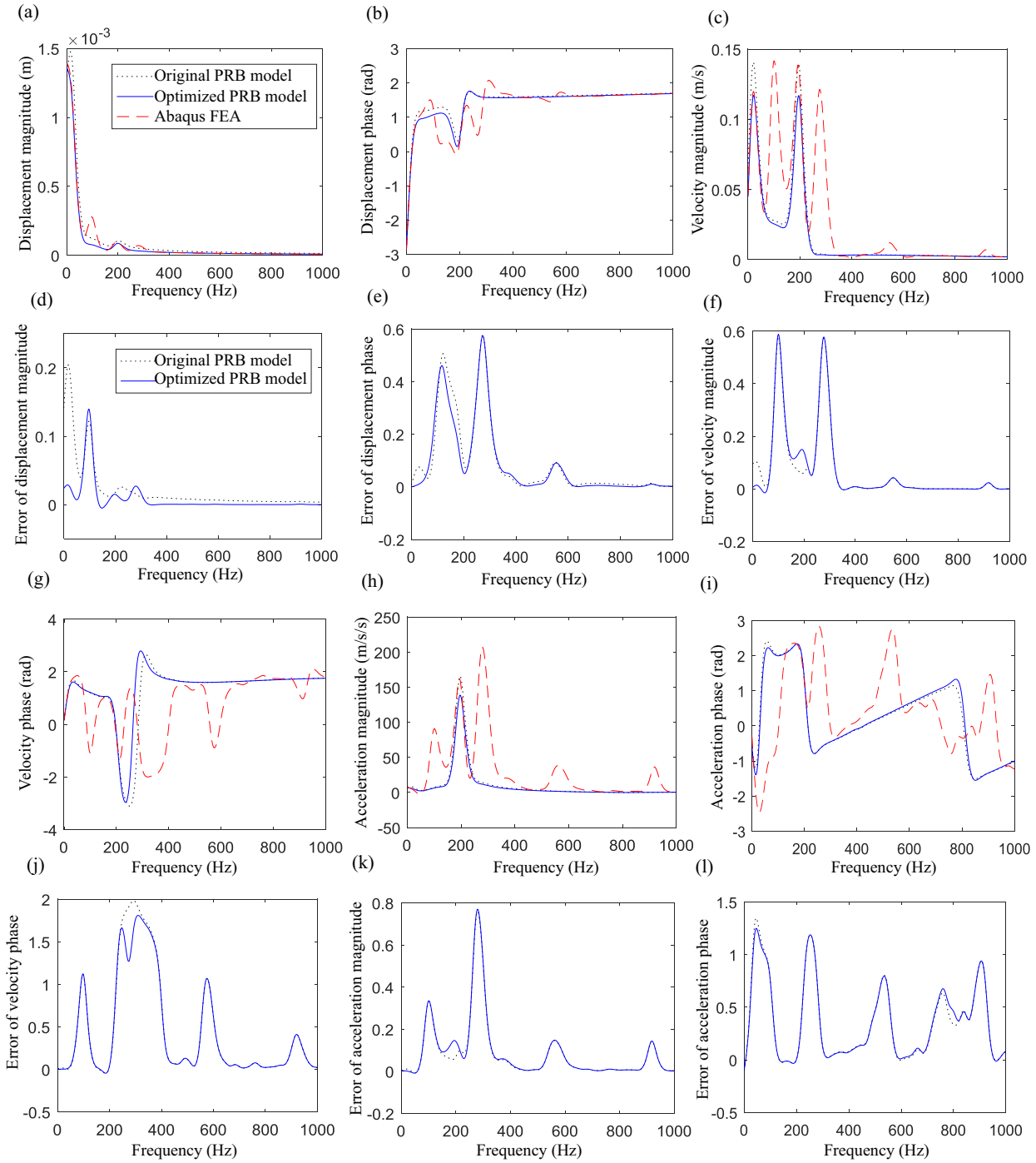

Fig. 13. The frequency domain analysis of the displacement response of the pinned-root compliant parallel-guiding mechanism at $A = 10$ N, $\omega = 200$ Hz, and $\lambda = 0$. (a) and (d) represent the magnitude of the displacement and the associated error, (b) and (e) represent the phase of the displacement and the associated error, (c) and (i) represent the magnitude of the velocity and the associated error, (g) and (j) represent the phase of the velocity and the associated error, (h) and (k) represent the magnitude of the acceleration and the associated error, (i) and (l) represent the phase of the acceleration and the associated error.

accuracy. It should be pointed out that the proposed PRB models are limited to predict dynamics of compliant mechanisms at relatively low frequencies. To overcome this limit, one may seek to use higher order PRB models, such as 2R/3R or RPR which can capture more complex mode shapes. However, this will increase the complexity of modeling and computational time. Obviously, a trade-off may be needed by considering the specific applications and allowable computational complexity.

Acknowledgments

The first author would like to thank Dr. Yuan Zheng from Department of Electrical and Computer Engineering of The Ohio State University for his advice on the frequency domain analysis. This material is based upon work supported by the National Science Foundation under Grant no: CMMI-1637656. Any opinions, findings, and conclusions or recommendations expressed in this material are those of the author(s) and do not necessarily reflect the views of the funding agencies.

Appendix A. Data tables

Table 5
The values of y_i of the fixed-guided compliant beam.

	y_1	y_2	y_3
0	2.36502016	5.497803918	8.639379828
0.1	2.234921325	5.294377883	8.352696295
0.2	2.133388562	5.174338293	8.215369244
0.3	2.051021398	5.095861203	8.136411803
0.4	1.982246093	5.040735505	8.08544728
0.5	1.923535651	4.999952882	8.049920375
0.6	1.872536832	4.968586228	8.023771431
0.7	1.827611373	4.943724215	8.003733644
0.8	1.787577069	4.923539778	7.987895072
0.9	1.751556337	4.906829718	7.975064113
1	1.718881343	4.892770007	7.964460128
5	1.22252097	4.768900303	7.877996202
10	1.037125321	4.749948383	7.865777068
100	0.588020867	4.732076443	7.85447814
1000	0.330944365	4.730244774	7.85333214
1.00E+04	0.186119244	4.730061152	7.853217377
1.00E+05	0.104663417	4.730042786	7.853205899
1.00E+06	0.058856614	4.730040949	7.853204751

Table 6
Validation of the continuum model of the fixed-guided compliant beam.

λ	Continuum model			FEA simulation			Errors (%)		
	${}^{c}f_1$	${}^{c}f_2$	${}^{c}f_3$	${}^{s}f_1$	${}^{s}f_2$	${}^{s}f_3$	δ_1	δ_2	δ_3
0	25.66119628	138.6708772	342.4303674	25.735	139.13	343.99	0.2868	0.33	0.4534
0.1	22.91561992	128.5988269	320.0813496	22.982	129.03	321.55	0.2888	0.3342	0.4567
0.2	20.88079648	122.833485	309.6429633	20.941	123.25	311.08	0.2875	0.3379	0.462
0.3	19.29956492	119.1358086	303.719711	19.356	119.54	305.13	0.2916	0.3381	0.4622
0.4	18.02694666	116.572189	299.9267732	18.079	116.97	301.33	0.2879	0.3401	0.4657
0.5	16.97491444	114.6935405	297.2968481	17.024	115.08	298.69	0.2883	0.3358	0.4664
0.6	16.08673373	113.2590197	295.3685395	16.134	113.65	296.75	0.293	0.344	0.4655
0.7	15.32409514	112.1283953	293.8951305	15.369	112.51	295.27	0.2922	0.3392	0.4656
0.8	14.66009166	111.2146598	292.7331045	14.703	111.6	294.11	0.2918	0.3453	0.4682
0.9	14.07522535	110.4610353	291.7934252	14.116	110.84	293.16	0.2889	0.3419	0.4662
1	13.55498156	109.8289265	291.0179791	13.595	110.21	292.39	0.2944	0.3458	0.4692
5	6.85677297	104.3382678	284.7335677	6.877	104.7	286.08	0.2941	0.3455	0.4706
10	4.934800618	103.5106215	283.850983	4.9494	103.87	285.19	0.295	0.346	0.4695
100	1.586326618	102.7331581	283.0360837	1.591	103.09	284.37	0.2937	0.3461	0.4691
1000	0.502478077	102.6536427	282.9534975	0.50396	103.01	284.29	0.2941	0.3459	0.4701
1.00E+04	0.158924075	102.6456731	282.9452278	0.15939	103	284.28	0.2923	0.344	0.4695
1.00E+05	0.050257045	102.6448759	282.9444007	5.04E−02	103	284.28	0.2947	0.3448	0.4698
1.00E+06	0.0158927	102.6447962	282.944318	1.59E−02	103	284.28	0.2949	0.3449	0.4698

Table 7
The values of y_i of the pinned-guided compliant beam.

	y_1	y_2	y_3
0	1.57079633	4.712385615	7.853981632
0.1	1.50065129	4.529774083	7.585629476
0.2	1.44363188	4.415150673	7.45046102
0.3	1.39593031	4.336902032	7.370479808
0.4	1.35514076	4.280178821	7.317920785
0.5	1.31965717	4.237201797	7.280835152
0.6	1.28835958	4.203525157	7.25329995
0.7	1.26043896	4.176429021	7.23206107
0.8	1.23529352	4.154158486	7.215187259
0.9	1.21246462	4.135530949	7.201461759
1	1.19159535	4.11972071	7.190080574
5	0.8599234	3.974544393	7.095988284
10	0.73135369	3.951317609	7.082504606
100	0.41567528	3.929144862	7.069995179
1000	0.23400632	3.9268573	7.068724194
1.00E+04	0.1316058	3.926627818	7.068596893
1.00E+05	0.07400819	3.926604863	7.06858416
1.00E+06	0.04161791	3.926602567	7.068582887

Table 8
Validation of the continuum model of the pinned-guided compliant beam.

λ	Continuum model			FEA simulation			Errors (%)		
	${}^{c}f_1$	${}^{c}f_2$	${}^{c}f_3$	${}^{s}f_1$	${}^{s}f_2$	${}^{s}f_3$	δ_1	δ_2	δ_3
0	11.32001207	101.8799631	283.0003015	11.352	102.31	284.6	0.2818	0.4203	0.5621
0.1	10.33157921	94.13697119	263.9917686	10.362	94.534	265.5	0.2936	0.42	0.5681
0.2	9.561368612	89.43308124	254.667444	9.5895	89.811	256.13	0.2934	0.4208	0.571
0.3	8.939940171	86.29117035	249.2290472	8.9666	86.656	250.66	0.2973	0.421	0.5709
0.4	8.425117259	84.04869277	245.6872073	8.4505	84.405	247.1	0.3004	0.4221	0.5717
0.5	7.989679827	82.36931065	243.2033383	8.0139	82.718	244.61	0.3022	0.4215	0.5751
0.6	7.615200098	81.06519607	241.367288	7.6384	81.409	242.76	0.3037	0.4223	0.5737
0.7	7.288711674	80.02346374	239.9558296	7.311	80.362	241.34	0.3049	0.4213	0.5735
0.8	7.000796666	79.17229943	238.8374082	7.0223	79.507	240.22	0.3062	0.421	0.5756
0.9	6.744430552	78.46386306	237.9295885	6.7652	78.796	239.31	0.307	0.4215	0.5768
1	6.51425467	77.86507121	237.1781352	6.5344	78.194	238.55	0.3083	0.4207	0.5751
5	3.392553192	72.47393465	231.0111357	3.4034	72.779	232.35	0.3187	0.4192	0.5762
10	2.453929336	71.62935088	230.1340428	2.4618	71.93	231.47	0.3197	0.418	0.5772
100	0.792712175	70.82771278	229.3218153	0.79527	71.124	230.65	0.3216	0.4166	0.5758
1000	0.251224688	70.7452645	229.2393716	0.25204	71.042	230.57	0.3235	0.4177	0.5771
1.00E+04	0.079461584	70.73699618	229.2311149	7.97E−02	71.033	230.56	0.3218	0.4167	0.5764
1.00E+05	0.025128508	70.73616911	229.2302891	2.52E−02	71.032	230.56	0.3217	0.4165	0.5767
1.00E+06	0.007946349	70.7360864	229.2302065	7.97E−03	71.032	230.56	0.3219	0.4166	0.5768

Table 9
Optimization results for the fixed-guided compliant beam.

λ	Continuum	The original PRB model		The optimized PRB model				
	${}^{c}f_1$	${}^{p}f_1$	$\bar{\delta}_1$ (%)	β_2	β_3	α_2	${}^{p}f_1$	$\bar{\delta}_1$(%)
0	25.66119	27.2177	6.065619	0.824542	0.100458	0.532669	25.66119	1.54E−07
0.1	22.91562	24.06602	5.020173	0.823175	0.101825	0.534399	22.91562	3.69E−08
0.2	20.8808	21.80461	4.424217	0.821281	0.103719	0.536818	20.8808	1.42E−08
0.3	19.29956	20.08039	4.045817	0.819091	0.105909	0.539624	19.29956	7.27E−09
0.4	18.02695	18.70962	3.786942	0.816718	0.108282	0.542669	18.02695	4.52E−09
0.5	16.97492	17.586	3.59993	0.814226	0.110774	0.54587	16.97492	3.22E−09
0.6	16.08673	16.6432	3.459147	0.811651	0.113349	0.549181	16.08673	2.56E−09
0.7	15.3241	15.8374	3.349645	0.809017	0.115983	0.552571	15.3241	2.19E−09
0.8	14.66009	15.13834	3.262255	0.80634	0.11866	0.55602	14.66009	2.02E−09
0.9	14.07523	14.52437	3.191009	0.803628	0.121372	0.559514	14.07523	1.96E−09
1	13.55498	13.97951	3.131885	0.800891	0.124109	0.563045	13.55498	1.96E−09
5	6.856773	7.038501	2.650349	0.687381	0.237619	0.714816	6.856773	4.17E−12
10	4.934801	5.062326	2.584209	0.566106	0.358894	0.934659	4.934801	9.55E−10
100	1.586327	1.626366	2.524045	0	1	1	1.621125	2.193636
1000	0.502478	0.515131	2.518006	0	1	1	0.514963	2.484716
1.00E+04	0.158924	0.162925	2.517401	0	1	1	0.16292	2.514301
1.00E+05	0.050257	0.051522	2.517341	0	1	1	0.051522	2.517341
1.00E+06	0.015893	0.016293	2.517334	0	1	1	0.016293	2.517334

Table 10
Optimization results for the pinned-guided compliant beam.

λ	Continuum	The original PRB model		The optimized PRB model				
	${}^{c}f_1$	${}^{P}f_1$	$\bar{\delta}_1$ (%)	β_1	β_2	α_1	${}^{P}f_1$	$\bar{\delta}_1$(%)
0	11.32001	12.37525	9.32189	0.802277	0.197723	0.561906	11.32001	4.71E−13
0.1	10.33158	11.1549	7.968979	0.800067	0.199933	0.564686	10.33158	2.06E−13
0.2	9.561369	10.23644	7.060393	0.797664	0.202336	0.567744	9.561369	1.90E−08
0.3	8.93994	9.512931	6.409339	0.795139	0.204861	0.570977	8.93994	2.35E−07
0.4	8.425117	8.923921	5.920431	0.792534	0.207466	0.574326	8.425117	1.38E−07
0.5	7.98968	8.432312	5.540052	0.789873	0.210127	0.577757	7.98968	9.03E−08
0.6	7.6152	8.013917	5.235806	0.787171	0.212829	0.581249	7.6152	6.56E−08
0.7	7.288712	7.652199	4.986986	0.784439	0.215561	0.584787	7.288712	5.19E−08
0.8	7.000797	7.335417	4.779753	0.781683	0.218317	0.588361	7.000797	4.43E−08
0.9	6.744431	7.054979	4.604511	0.77891	0.22109	0.591965	6.744431	4.03E−08
1	6.514255	6.804426	4.454399	0.776122	0.223878	0.595594	6.514255	3.85E−08
5	3.392553	3.494877	3.01613	0.66631	0.33369	0.752012	3.392553	5.37E−10
10	2.453929	2.522049	2.775944	0.577148	0.422852	0.975907	2.453929	1.74E−12
100	0.792712	0.812879	2.544083	0	1	1	0.810262	2.213854
1000	0.251225	0.257556	2.520019	0	1	1	0.257472	2.48673
1.00E+04	0.079462	0.081462	2.517604	0	1	1	0.08146	2.514504
1.00E+05	0.025129	0.025761	2.51736	0	1	1	0.025761	2.51736
1.00E+06	0.007946	0.008146	2.51734	0	1	1	0.008146	2.51734

Table 11
Validation of the fundamental frequency of the fixed-guided compliant beam and fixed-root compliant parallel-guiding mechanism.

Models	Fundamental natural frequency of the fixed-guided compliant beam (Hz)				Fundamental natural frequency of the fixed-root compliant parallel-guiding mechanisms (Hz)		
	Theoretical original PRB model	Theoretical optimized PRB model	Theoretical continuum model	Abaqus FEA	ADAMS original PRB model	ADAMS optimized PRB model	Abaqus FEA
$\lambda_1 = 0$	27.2177	25.66119	25.66119	25.735	27.0997	25.5127	25.69
$\lambda_2 = 0.5$	17.586	16.97492	16.97492	17.024	17.4729	17.0299	17.012
$\lambda_3 = 10$	5.0623	4.934801	4.934801	4.9494	5.188	4.9801	4.9447

Table 12
Validation of the fundamental frequency of the pinned-guided compliant beam and pinned-root compliant parallel-guiding mechanism.

Models	Fundamental natural frequency of the pinned-guided compliant beam (Hz)				Fundamental natural frequency of the pinned-root compliant parallel-guiding mechanisms (Hz)		
	Theoretical original PRB model	Theoretical optimized PRB model	Theoretical continuum model	Abaqus FEA	ADAMS original PRB model	ADAMS optimized PRB model	Abaqus FEA
$\lambda_1 = 0$	12.37525	11.32001	11.32001207	11.352	12.4207	11.3831	11.393
$\lambda_2 = 0.5$	8.432312	7.98968	7.989679827	8.0139	8.4534	8.0892	8.0407
$\lambda_3 = 10$	2.522049	2.453929	2.453929336	2.4618	2.5636	2.471	2.468

Supplementary material

Supplementary material associated with this article can be found, in the online version, at 10.1016/j.mechmachtheory.2018.04.005.

References

[1] J. Qiu, J.H. Lang, A.H. Slocum, A curved-beam bistable mechanism, J. Microelectromech. Syst. 13 (2) (2004) 137–146.
[2] S. Kota, K.-J. Lu, Z. Kreiner, B. Trease, J. Arenas, J. Geiger, Design and application of compliant mechanisms for surgical tools, J. Biomech. Eng. 127 (6) (2005) 981–989.
[3] Y. She, C.J. Hurd, H.-J. Su, A transformable wheel robot with a passive leg, in: Intelligent Robots and Systems (IROS), 2015 IEEE/RSJ International Conference on, IEEE, 2015, pp. 4165–4170.
[4] B.H. Kang, J.-Y. Wen, N.G. Dagalakis, J.J. Gorman, Analysis and design of parallel mechanisms with flexure joints, IEEE Trans. Rob. 21 (6) (2005) 1179–1185.
[5] Y. She, H.-J. Su, D. Meng, S. Song, J. Wang, Design and modeling of a compliant link for inherently safe corobots, J. Mech. Robot. 10 (1) (2018) 011001.
[6] Y. She, H.-J. Su, C. Lai, D. Meng, Design and prototype of a tunable stiffness arm for safe human-robot interaction, in: ASME 2016 International Design Engineering Technical Conferences and Computers and Information in Engineering Conference, American Society of Mechanical Engineers, 2016, pp. V05BT07A063–V05BT07A063.
[7] L.L. Howell, S.P. Magleby, B.M. Olsen, Handbook of Compliant Mechanisms, John Wiley & Sons, 2013.
[8] N. Lobontiu, E. Garcia, Circular-hinge line element for finite element analysis of compliant mechanisms, Trans. Am. Soc. Mech. Eng. J. Mech. Des. 127 (4) (2005) 766.
[9] L.L. Howell, A. Midha, A method for the design of compliant mechanisms with small-length flexural pivots, J. Mech. Des. 116 (1) (1994) 280–290.

[10] L.L. Howell, A. Midha, T. Norton, Evaluation of equivalent spring stiffness for use in a pseudo–rigid–body model of large-deflection compliant mechanisms, J. Mech. Des. 118 (1) (1996) 126–131.
[11] F. Ma, G. Chen, Modeling large planar deflections of flexible beams in compliant mechanisms using chained beam-constraint-model, J. Mech. Robot. 8 (2) (2016) 021018.
[12] O.A. Turkkan, H.-J. Su, A general and efficient multiple segment method for kinetostatic analysis of planar compliant mechanisms, Mech. Mach. Theory 112 (2017) 205–217.
[13] Y.-Q. Yu, Z.-L. Feng, Q.-P. Xu, A pseudo–rigid–body 2r model of flexural beam in compliant mechanisms, Mech. Mach. Theory 55 (2012) 18–33.
[14] H.-J. Su, A pseudo-rigid-body 3r model for determining large deflection of cantilever beams subject to tip loads, J. Mech. Robot. 1 (2) (2009) 021008.
[15] V.K. Venkiteswaran, H.-J. Su, A three-spring pseudo-rigid-body model for soft joints with significant elongation effects, J. Mech. Robot. 8 (6) (2016) 061001.
[16] V.K. Venkiteswaran, H.-J. Su, Pseudo–Rigid–Body models for circular beams under combined tip loads, Mech. Mach. Theory 106 (2016) 80–93.
[17] J.E. McInroy, J.C. Hamann, Design and control of flexure jointed hexapods, IEEE Trans. Robot. Autom. 16 (4) (2000) 372–381.
[18] N. Lobontiu, Compliant Mechanisms: Design of Flexure Hinges, CRC Press, 2002.
[19] Z. Li, S. Kota, Dynamic analysis of compliant mechanisms, in: Proceedings of the ASME Design Engineering Technical Conference, Vol. 5, 2002, pp. 43–50.
[20] M. Rösner, R. Lammering, R. Friedrich, Dynamic modeling and model order reduction of compliant mechanisms, Precis. Eng. 42 (2015) 85–92.
[21] H. Zhao, S. Bi, B. Pan, Dynamic analysis and experiment of a novel ultra-precision compliant linear-motion mechanism, Precis. Eng. 42 (2015) 352–359.
[22] C. Boyle, L.L. Howell, S.P. Magleby, M.S. Evans, Dynamic modeling of compliant constant-force compression mechanisms, Mech. Mach. Theory 38 (12) (2003) 1469–1487.
[23] Y.-Q. Yu, L.L. Howell, C. Lusk, Y. Yue, M.-G. He, Dynamic modeling of compliant mechanisms based on the pseudo–rigid–body model, J. Mech. Des. 127 (4) (2005) 760–765.
[24] S.M. Lyon, M.S. Evans, P.A. Erickson, L. Howell, Dynamic response of compliant mechanisms using the pseudo–rigid–body model, in: Proceedings of, 1997.
[25] S. Lyon, P. Erickson, M. Evans, L. Howell, Prediction of the first modal frequency of compliant mechanisms using the Pseudo–Rigid–Body model, J. Mech. Des. 121 (2) (1999) 309–313.
[26] Y. She, D. Meng, H. Shi, H.-J. Su, Dynamic modeling of a 2d compliant link for safety evaluation in human-robot interactions, in: Intelligent Robots and Systems (IROS), 2015 IEEE/RSJ International Conference on, IEEE, 2015, pp. 3759–3764.
[27] Y. She, D. Meng, H.-J. Su, Pseudo–Rigid–Body models for dynamics of compliant robotic links, in: ASME 2017 International Design Engineering Technical Conferences and Computers and Information in Engineering Conference, American Society of Mechanical Engineers, 2017 , pp. V05AT08A032–V05AT08A032.
[28] N. Li, H.-J. Su, X.-P. Zhang, Accuracy assessment of pseudo–rigid–body model for dynamic analysis of compliant mechanisms, J. Mech. Robot. 9 (5) (2017) 054503.
[29] L.L. Howell, Compliant Mechanisms, John Wiley & Sons, 2001.
[30] M.L. Culpepper, C.M. DiBiasio, R.M. Panas, S. Magleby, L.L. Howell, Simulation of a carbon nanotube-based compliant parallel-guiding mechanism: a nanomechanical building block, Appl. Phys. Lett. 89 (20) (2006) 203111.
[31] W.C. Tang, T.-C.H. Nguyen, R.T. Howe, Laterally driven polysilicon resonant microstructures, Sens. Actuators 20 (1–2) (1989) 25–32.
[32] P. Laura, J. Pombo, E. Susemihl, A note on the vibrations of a clamped-free beam with a mass at the free end, J. Sound Vib. 37 (2) (1974) 161–168.
[33] M.W. Spong, M. Vidyasagar, Robot Dynamics and Control, John Wiley & Sons, 2008.
[34] S. Briot, W. Khalil, et al., Dynamics of Parallel Robots, Springer, 2015.